HASP Student Payload Application for 2022

Payload Title: GASP [Generalized Aerosol Sampling Payload]

Institution: University of Maryland

Payload Class (Enter SMALL, or LARGE): LARGE	**Submit Date:** 01/07/2022

Project Abstract:
Atmospheric radionuclides of beryllium, *7Be* and *10Be*, are readily produced in the stratosphere from cosmic ray collisions with heavier nuclei. Once produced, they are adsorbed onto ambient aerosols. These aerosols accumulate *10Be* and *7Be* throughout their stratospheric residency until they are transported to the troposphere where they are quickly removed by scavenging or deposition. Due to the short half-life of *7Be* (53 days) with respect to *10Be* (1.4M years), *10Be/7Be* in aerosols is highly sensitive to stratospheric residence time and is thus a powerful tracer of air mass transport and stratosphere-troposphere exchange (STE). However, the low abundance of these isotopes has restricted *in-situ* atmospheric collections to aircraft campaigns capable of sampling large air volumes at low altitudes (<12km). Similarly, the logistics of counting numerous low-level *7Be* samples from a single campaign has limited creation of the large spatial datasets needed for event-based applications. To overcome these limitations, we apply a new accelerator mass spectrometry (AMS) capability recently developed at Lawrence Livermore National Laboratory (LLNL) which requires as little as 10^4 atoms of either isotope, and minimal sample preparation. This technique is used here on a University of Maryland (UMD) designed Generalized Aerosol Sampling Payload (GASP) built for high-altitude balloon missions. As a payload on CSBF-HASP, GASP will investigate large-scale dynamic drivers of STE events, including mountain-generated gravity waves and subsequent mixing and dynamics in the stratosphere. Applications of these data range from an improved understanding of stratospheric turbulence for aircraft applications to climate-related processes.

Team Name: UMD NearSpace	**Team or Project Website:** https://bpp.umd.edu/ http://www.hyper.umd.edu/

	Student Leader Contact Information:	**Faculty Advisor Contact Information:**
Name:	Mathew Killian	Dr. Mary Bowden
Department:	Aerospace Engineering	Aerospace Engineering
Mailing Address:	3179 Glenn L. Martin Hall 4298 Campus Drive University of Maryland	3179 Glenn L. Martin Hall 4298 Campus Drive University of Maryland
City, State, Zip code:	MD, 20742	MD, 20742
e-mail:	mkillian@umd.edu	bowden@umd.edu
Office Telephone:	-	-
Mobile Telephone:	201-996-6792	301-275-7723

HASP Student Payload Application for 2022

Flight Hazard Certification Checklist

NASA has identified several classes of material as hazardous to personnel and/or flight systems. This checklist identifies these documented risks. Applying flight groups are required to acknowledge if the payload will include any of the hazards included on the list below. Simply place an (x) in the appropriate field for each hazard classification. **Note:** Certain classifications are explicitly banned from HASP (grey filled items on table below) and the remaining hazards will require additional paperwork and certifications. If you intend to include one of the hazards, you must include detailed documentation in section 3.8 of the application as required by the HASP Call for Payloads.

This certification must be signed by both the team faculty advisor and the student team lead and included in your application immediately following the cover sheet form.

Hazardous Materials List

Classification	Included on Payload	Not Included on Payload
RF transmitters		X
High Voltage		X
Lasers (Class 1, 2, and 3R only) Fully Enclosed	X	
Intentionally Dropped Components		X
Liquid Chemicals		X
Cryogenic Materials		X
Radioactive Material		X
Pressure Vessels		X
Pyrotechnics		X
Magnets less than 1 Gauss		X
UV Light		X
Biological Samples		X
Batteries	X	
High intensity light source		X

Student Team Leader Signature: ______________________

Faculty Advisor Signature: ______________________

Generalized Aerosol Sampling Payload

University of Maryland HASP 2022 Payload Proposal

Submission Date: January 7^{th}, 2022

–

UMD Balloon Payload Program [BPP]
Space Systems Laboratory [SSL]
Hypersonic Aerodynamics and Propulsion Laboratory [HAPL]
University of Maryland, College Park
Department of Aerospace Engineering
–
Lawrence Livermore National Laboratory [LLNL]

Funding provided by Lawrence Livermore National Laboratory

Contents

1 Abstract

Atmospheric radionuclides of beryllium, $7Be$ and $10Be$, are readily produced in the stratosphere from cosmic ray collisions with heavier nuclei. Once produced, they are adsorbed onto ambient aerosols. These aerosols accumulate $10Be$ and $7Be$ throughout their stratospheric residency until they are transported to the troposphere where they are quickly removed by scavenging or deposition. Due to the short half-life of $7Be$ (53 days) with respect to $10Be$ ($1.4M$ years), $10Be/7Be$ in aerosols is highly sensitive to stratospheric residence time and is thus a powerful tracer of air mass transport and stratosphere-troposphere exchange (STE). However, the low abundance of these isotopes has restricted *in-situ* atmospheric collections to aircraft campaigns capable of sampling large air volumes at low altitudes ($< 12km$). Similarly, the logistics of counting numerous low-level $7Be$ samples from a single campaign has limited creation of the large spatial datasets needed for event-based applications. To overcome these limitations, we apply a new accelerator mass spectrometry (AMS) capability recently developed at Lawrence Livermore National Laboratory (LLNL) which requires as little as 10^4 atoms of either isotope, and minimal sample preparation. This technique is used here on a University of Maryland (UMD) designed Generalized Aerosol Sampling Payload (GASP) built for high-altitude balloon missions. As a payload on CSBF-HASP, GASP will investigate large-scale dynamic drivers of STE events, including mountain-generated gravity waves and subsequent mixing and dynamics in the stratosphere. Applications of these data range from an improved understanding of stratospheric turbulence for aircraft applications to climate-related processes.

2 Payload Overview

2.1 Payload Scientific and Technical Motivation

Transition from laminar to turbulent flow in the boundary layers on the surface of a hypersonic flight vehicle (HFV) brings with it a number of detrimental effects: a marked increase in surface heating levels (see Figure 1), elevated frictional drag, and large-amplitude pressure fluctuations that can couple with the structure of the vehicle and produce undesired oscillations. The prediction of transition in flight is thus of crucial importance in the vehicle design process. Transition is a highly complicated phenomenon and can follow several paths, depending on the intensity of the disturbance environment [2]. The conventional sequence for low-disturbance environments has freestream disturbances (vorticity, sound, and/or entropy spots) exciting normal modes within the boundary-layer through receptivity; these modes initially undergo linear growth until their amplitudes are sufficiently large that nonlinear effects take over, eventually resulting in the formation of turbulent spots. These then merge to produce a fully turbulent boundary-layer. While substantial progress has been made recently in understanding parts of this sequence and the overall transition process using theory, numerical simulations, and ground testing, extrapolation to flight requires knowledge of the ambient flow disturbance environment likely to be encountered by hypersonic vehicles.

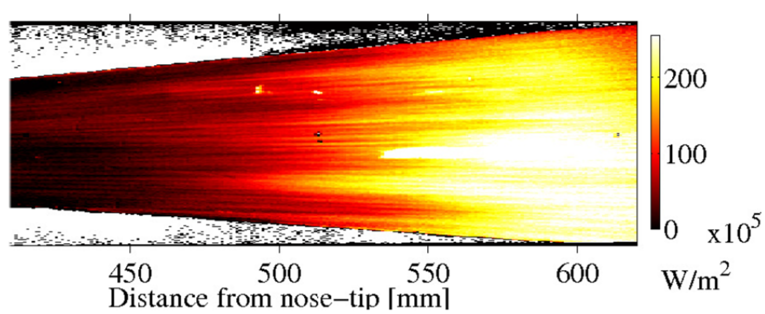

Figure 1: Heat-flux distribution measured on the surface of a slender cone at Mach 7.5 [1]. The marked increase in heat flux is caused by transition to turbulence of the boundary layer.

In 1976, Reshotko's [2] review article on boundary-layer stability and transition expressed pessimism regarding the prediction of transition in flight due to the lack of information of the disturbance environment at relevant altitudes. Hypersonic flight will typically take place in the range of 24-60km ($\approx$ 80-200kft), *i.e.*, in the upper stratosphere and lower mesosphere. Such altitudes are generally beyond the limits accessible by aircraft-based measurement; for example, the U2-based HICAT program [3] was restricted to 70kft, NASA's ER-2 aircraft is mostly restricted to fly science missions below 70kft, the SR-71 Blackbird was capable of altitudes up to 90kft [4, 5], and more recently the Perlan-Airbus high altitude glider reached 76kft in September 2018 [6, 7]. In the years since Reshotko [2], however, a number of balloon- and sounding-rocket-based measurements have probed the upper atmosphere: balloons are able to achieve altitudes typically in the range of 80-150kft [8, 9, 10, 11, 12], while sounding rockets are used for higher altitudes [13]. Previous measurements have primarily been carried out by atmospheric physicists, with the intent of obtaining geophysical information regarding clear air turbulence (CAT) at these altitudes. Only recently have measurements focused on the small length scales (millimeters to centimeters) of turbulence characteristic of hypersonic boundary layers and thus of relevance to the transition process. For example, Skinner et al. [14], at the University of Maryland (UMD), have developed FiSH to examine turbulent velocity, vorticity, temperature, and high frequency acoustic fluctuation (up to $25kHz$) properties simultaneously, down to millimeter length-scales in the stratosphere with a payload that can operate for extended periods of time. Preliminary flights at 30km show promising turbulence spectra information for HFV engineers.

Nevertheless, a clear gap remains in our knowledge of the ambient, global stratospheric turbulent environment to inform hypersonic boundary-layer transition predictions. Misinterpreted freestream disturbances can result in markedly enhanced thermal and mechanical loads compared to predictions (or alternatively, an over-designed thermal protection system) if not appropriately understood and taken into consideration for robust vehicle design. The US Air-Force recently commented that an incomplete understanding of the flight atmosphere at relevant altitudes is what partially led to recent hypersonic flight-test failures (e.g. DARPA's Hypersonic Technology Vehicle (HTV-2) failed because of unexpected heat stress due to high sensitivity to atmospheric disturbances).

In addition to *in-situ* measurements of turbulence, temperature, pressure, and wind, aerosol measurements are also needed to fully characterize the flight environment as they too serve as disturbance events. Furthermore, to forecast the flight environment and its potential disturbance modes, an improved understanding of the dynamic processes in the stratosphere, including stratosphere-troposphere exchange (STE), is critically needed. With this in mind, a new particle collector for obtaining stratospheric samples of radionuclides of beryllium - the Generalized Aerosol Sampling Payload, or GASP - has been designed, fabricated and flown by students at the University of Maryland on sounding balloon flights. Here we will refer to the sounding balloon variant of GASP as '*wee*-GASP', and the zero-pressure balloon variant as 'HASP-GASP'.

Beryllium attaches to naturally occurring aerosols in the stratosphere and can be collected on a filter membrane given that enough air, at these high altitudes, is pumped through it to obtain a detectable concentration. This prior limitation to balloon flight measurements is solved here using GASP and LLNL's Center for Accelerator Mass Spectrometry (CAMS) facility, a state-of-the-art AMS for ultra-sensitive isotope ratio measurements. Here, we use two radionuclides of beryllium, $10Be$ and $7Be$, as an atmospheric tracer for capturing some of the larger-scale dynamical processes controlling vertical and horizontal motions and mixing in the stratosphere. This has the potential to better understand the dynamics that produce stratospheric turbulence, including mountain-generated gravity waves, which we hope to capture on the HASP flight. These dynamics will be simulated, and ultimately forecasted, using the Weather Research and Forecasting (WRF) model, and multi-physics variable density flow solver (VIDA) model that can resolve turbulence down to the sub-millimeter scale.

Furthermore, GASP measurements will identify the origin of the sampled air masses in the stratosphere as the ratio of $10Be/7Be$ depends on the amount of time the airmass has spent in the polar regions where the radionuclides are produced by cosmic waves [15]. These data provide information on how the measured aerosol properties depend on origin and trajectory of stratospheric air masses. These applications of beryllium-7 and -10 have never been attempted before.

wee-GASP uses an AMETEK centrifugal pump to process air through a set of 3D-printed housings containing various membrane filter mediums for the purpose of collecting aerosols in the stratosphere. The pump was chosen to efficiently force a large mass flow rate of air, equivalent to about $1.0m^3$ (equivalent to $1.225kg$) of air at standard temperature and pressure (STP), in minutes (at altitudes up to $35km$). *wee*-GASP also utilizes a GPS antenna, accelerometers, gyroscopes, magnetometers, pressure sensors, humidity sensors, and thermocouples to provide robust atmospheric data at $5Hz$ for the ascent and float phases of the flight, and to ensure that samples are collected at the correct altitudes. Within the tubing for the pump, there is an in-house designed and fabricated mass-flow meter, allowing the mass flow rate to be actively monitored at any altitude. This allows the pump to optimize its RPM for the given ambient pressure.

The major changes from the design of *wee*-GASP to the design for this HASP payload are primarily related to payload scaling - *wee*-GASP can only effectively acquire 4 samples at altitude, while HASP-GASP will be able to collect up to 36. It is anticipated that HASP-GASP will collect 6 samples ahead of reaching float altitude, and subsequently acquire the remaining 30 during the float at $\approx 35km$. At this altitude, a single sample will take $\approx$ 20 minutes to process, meaning that HASP-GASP would need a 10 hour float window to collect all 30 samples. If accepted, HASP-GASP will provide the first beryllium samples collected at altitudes above $20km$. To date, *wee-GASP* has only collected aerosol samples up to $17km$ due to logistical difficulties of long duration floats with a latex sounding balloon. HASP-GASP will allow us to see whether or not $10Be/7Be$ can be used to identify areas in the mid to lower stratosphere with increased gravity wave activity and/or areas with high shear due to jet streams or deep convection, i.e., Kelvin-Helmholz instabilities. This would indicate mechanisms for producing strong turbulence at scales relevant to hypersonic vehicle flight.

A significant addition, that is facilitated by the mass and power budget of the HASP gondola, is the Handix Scientific Portable Optical Particle Spectrometer (POPS), which will provide complimentary information on the size of the aerosols *in-situ*. The objective of the HASP payload is to process $1.225kg$ of air (or $1m^3$ of air at STP) through the payload for 36 different filter membranes to collect enough tracer particles to allow for the detection of Beryllium isotopes. This mass/STP volume of air have been selected due to data from Jordan et al. [15] who indicates that $1m^3$ of ambient air from the ST boundary contains on the order of 10^6 atoms of $7Be$ and $10Be$. This amount would be a sufficient sample size. Although this will vary spatially, we only require 10^4 atoms contained within any given sample.

2.1.1 Mission Statement

Using HASP to ascend to $35-36$km and loiter for $10-20$ hours, the HASP-GASP payload will collect 30 aerosol samples along the flight path (in addition to 6 samples during ascent) and subsequently provide the first beryllium isotope samples collected at altitudes above 20 km to resolve dynamics associated with enhanced turbulence in the stratospheric flight environment.

2.1.2 Mission Background and Justification

When predicting and analyzing atmospheric conditions, it is important to track how air flows between distinct layers of the atmosphere. One of the most straightforward ways to do this is to identify tracer particles that can be measured to model stratospheric transport. Two candidate particles are beryllium isotopes $7Be$ and $10Be$, both of which are cosmogenic nuclides that are pervasive in the atmosphere [16]. These are generated by impacts of cosmic rays on nitrogen and oxygen atoms. One major benefit to using both isotopes is their difference in half-lives (1.4×10^6 years for $10Be$ and 53 days for $7Be$) which can tell us how old a certain airmass is after weather events. Additionally, it has been found that beryllium nuclides are produced nearly twice as much in the stratosphere as in the troposphere [17] and the concentration is one to two orders of magnitude higher in the stratosphere [18, 19], which can give a baseline for air content and origin at certain altitudes. The beryllium isotopes are measured using different techniques. While 7Be can be measured with gamma decay sensors, 10Be requires very precise accelerator mass spectrometry, which is much more difficult, but can be accomplished at LLNL-CAMS.

As air transports, the ratio between the beryllium isotopes also changes a measurable amount due to their vastly different half-lives. Both isotopes are associated with aerosols, so precipitation losses affect them roughly equally, which should not affect the ratio. It is known that measuring this beryllium ratio is effective in studying transport between the troposphere and stratosphere, more recently involving the processes through which the two layers exchange air [15]. Some of these mechanisms that are of particular interest include subtropical and polar jets, tropopause folding, and synoptic systems such as cyclones and northeasters, all of which cause interactions across the tropopause.

Jets and tropopause folds involve extruded air layers from the stratosphere which exchanges air in both directions across the tropopause. Weather systems like hurricanes generally only pull stratospheric air into the troposphere [20, 21]. While enough data has been collected to show the efficacy of using $10Be$ and $7Be$ as tracers, there is very little data regarding high-altitude observations of $10Be$. Most aerosol collection has been achieved on aircraft-based platforms, which limits sample acquisition to relatively low altitudes of 12 km or less [15, 22]. The theoretical highest production rate of beryllium isotopes occurs near the mid-stratosphere; the highest altitude recordings are from only 2.5 km above the tropopause [23, 24, 25]. The beryllium isotopes have also been incorporated in some atmospheric circulation models [16, 26, 27]. This has produced strong evidence of tropopausal exchange in mid-latitudes, which supports further experimentation [28].

In order to collect a substantial data set in the stratosphere, one would need to use an aircraft (e.g. NASA's ER-2 platform) or a zero-pressure balloon/aerostat able to reach high altitudes of interest ($> 20km$). A payload designed for this purpose could bear resemblance to the lightweight stratospheric air sampler LISA [29] and past University of Maryland payloads such as *wee*-GASP.

Over the last year, UMD has attempted beryllium collection on tandem sounding balloon flights that targeted float altitudes of about $24 - 28$km. Through several iterations of the design of GASP, our payload for aerosol collection, effective methods to pump air through 3D printed filter housings and obtain efficient collection has been identified. Sounding balloons burst at a much lower altitude than their zero-pressure counterparts and cannot carry as much weight, limiting the capabilities of *wee*-GASP. As such, it would be most effective to fly a dedicated, more robust payload on a zero-pressure platform, allowing us to acquire aerosol data that has thus far been out of reach.

2.1.3 Mission Objectives

- Use HASP-GASP for the collection of 36 discrete aerosol samples throughout the HASP flight, for analysis at Livermore's CAMS facility.
- Assess if the high mass flow rate air processing system works effectively.
- Assess if sufficient stratospheric samples of the beryllium radionuclides have been collected. A minimum sample requires a collections of at least $10,000$ Be atoms - of either isotope.
- Assess whether $10Be/7Be$ ratios can be used to identify regions exhibiting turbulence production. Can these ratios distinguish between gravity wave activity, high wind shear, deep convection, etc.?

These data will provide a foundation for future UMD/LLNL plans which are to combine *in-situ* turbulence measurement (using systems such as on FiSH) with GASP-measured beryllium tracers to allow us to identify the intensity of turbulence and the physical mechanisms producing turbulence in the stratosphere. We expect these to include the breaking of gravity waves or wind shear from high-altitude jets. This data will also provide information on how the measured aerosol properties depend on the origin and trajectory of stratospheric air masses. These applications of beryllium-7 and -10 have never been attempted before.

2.2 Payload Systems and Operation

A schematic for the HASP-GASP payload is presented in Figure 2. The internal layout of the payload is provided in Figure 3.

The main structural enclosure of the payload is an extruded Aluminium 6560 T-slotted frame which houses the science payload. This is enveloped in a Polyethylene thermal jacket for passive thermal regulation. The thermal jacket can be easily removed via reusable nylon push-in rivets with click lock shanks; this enables good access to all internal components. The base of the payload is secured to the PVC HASP mounting plate via 27 countersunk M4 bolts into the primary frame structure. Technical drawings for the payload are provided in Appendix B.

2.3 Major System Components

2.3.1 Sensors

A description of sensors, distributors, and part numbers are given in table 1. It is highlighted that the data acquisition system is composed of a network of three Arduino Mega boards acquiring data at $5Hz$. For a reference to how components are wired together refer to Figure 9. For the component layout within the HASP-GASP payload refer to Figure 3.

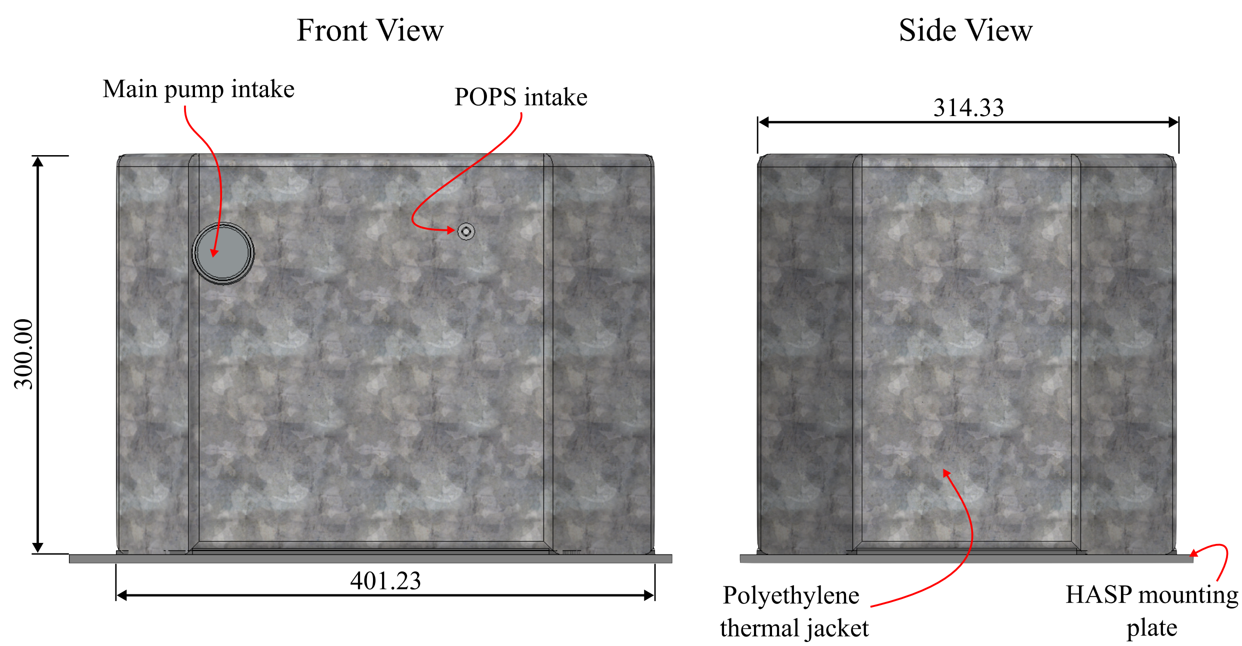

Figure 2: Schematic of HASP-GASP payload; dimensions in mm.

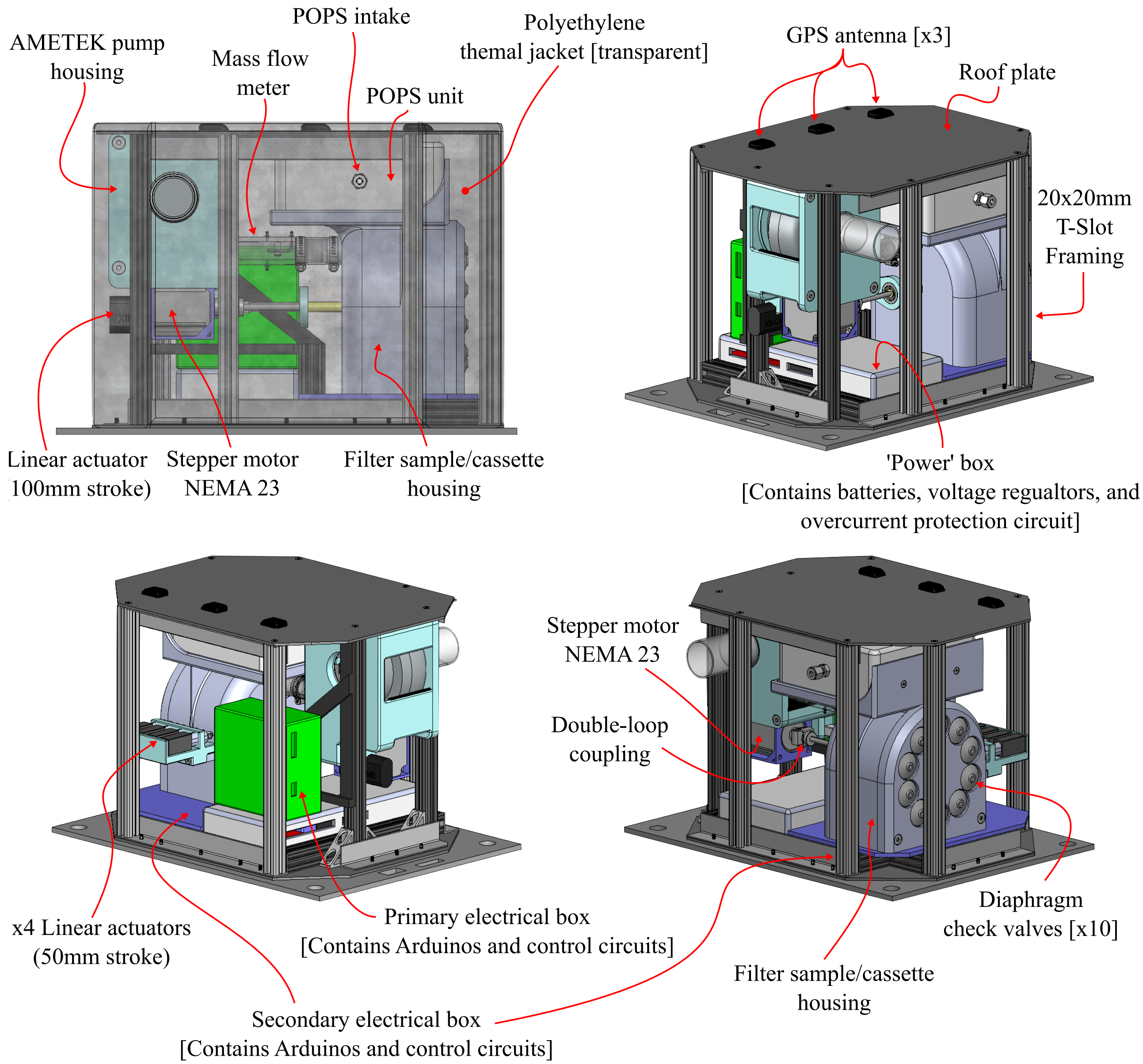

Figure 3: Schematic of HASP-GASP payload internal layout.

Part	Distributor	Quantity
Neo-6M GPS module	μblox	2
Pressure Transducer	Endevco, model 8515C-15	2
Thermocouple (K-type)	TC Direct, model 206-590	10
Thermocouple Amp	Adafruit, model MAX31856	10
Tri-axis Accelerometer	Adafruit, model LSM303	2
Temp, Pres, Humidity sensor	Adafruit, model BME280	3
Ported Pres sensor	Adafruit, model MPRLS	3
Voltage, Current, Power sensor	Adafruit, model INA260	12
Real Time clock	Adafruit, model DS3231	2
PCB differential Pres sensor	TE, model 4525DO-DS5AI001DP	4
Stepper motor encoder	McMaster Inc., model 6627T68	1

Table 1: Breakdown of HASP-GASP sensors.

2.3.2 Aerosol Collection System

The HASP-GASP payload is designed to make use of a rotating filter selection system that enables the appropriate filter to be aligned with the exhaust of the AMETEK centrifugal blower. The advantages of this are: 1) The flow path is minimized; 2) the flow path through the filters (in each cassette) is constant; 3) the flow path increases by a negligible $22mm$ between adjacent cassettes, and $88mm$ between cassette 1 and cassette 4; and 4) the flow path is straight. The HASP-GASP cassette actuation system is shown in Figure 4.

As shown in Figure 4, the cassette key is actuated by the 100mm stroke linear actuator to engage the appropriate cassette hole. Once the key is locked into place, the appropriate 50mm stroke linear actuator disengages the selected cassette so that it is free to rotate. Following this, the stepper motor rotates the cassette to align the selected filter with the flow path. Once aligned, the 50mm stroke actuator re-engages the cassette, locking it into place and preventing rotation while air is pumped through the filter medium.

An exploded view of the entire cassette housing assembly, holding 36 filter mediums, is presented in Figure 5. Note actuator shaft linkage connecting the stepper motor and the 100mm linear actuator to the cassette key. Cassette locking tabs are used to lock cassette rotationally as well as sense the angle of the cassette, once engaged with the appropriate 50mm linear actuator. The mechanism for this will be discussed further in Section 2.5.

An individual cassette assembly, containing 9 filter papers, is presented in Figure 6. The cassette assemblies will be printed from methacrylate photo-polymer resin, resulting in components having a matte white finish and a density of $2g/cm^3$, printed to a resolution of 50 microns. Similar, but smaller/individual filter sample housings are already used in *wee*-GASP sounding balloon flights and ground tests.

Individual filter papers are $25mm$ in diameter, and will be composed of several mediums. Membrane filter mediums of interest are: Nucleopore, Millipore, Cellulose, Polytetrafluoroethylene (PTFE), and QMA-quartz. Various membrane porosity is also of interest. These filters are mounted onto a support structure and then pinned circumferentially into place via a Buna-N square profile O-ring compressed down via an 8-pin bayonet lock filter inlet (identical to that already used in *wee*-GASP). The front face of the cassette is then lined with 9 individual filter Buna-N gaskets, while the exhaust side is lined with a PTFE Teflon gasket. When the cassettes are stacked (as shown in Figures 4 and 5) the Buna-N gaskets mate with the PTFE gaskets creating an airtight seal while allowing the cassette to rotate with moderate-to-low resistance.

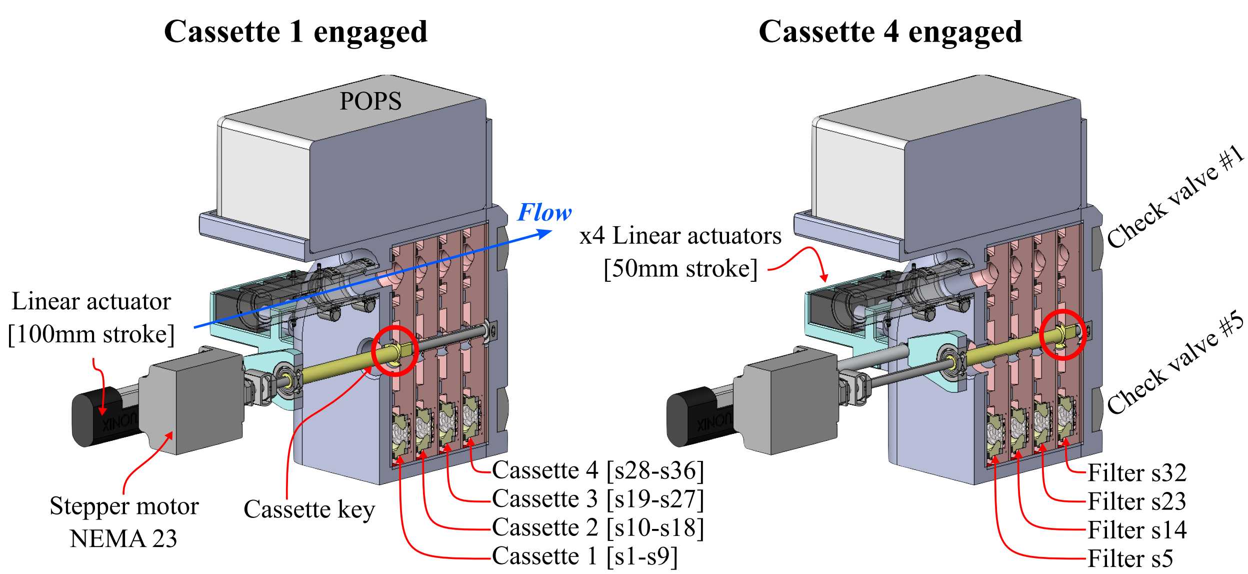

Figure 4: HASP-GASP cassette actuation and filter selection system.

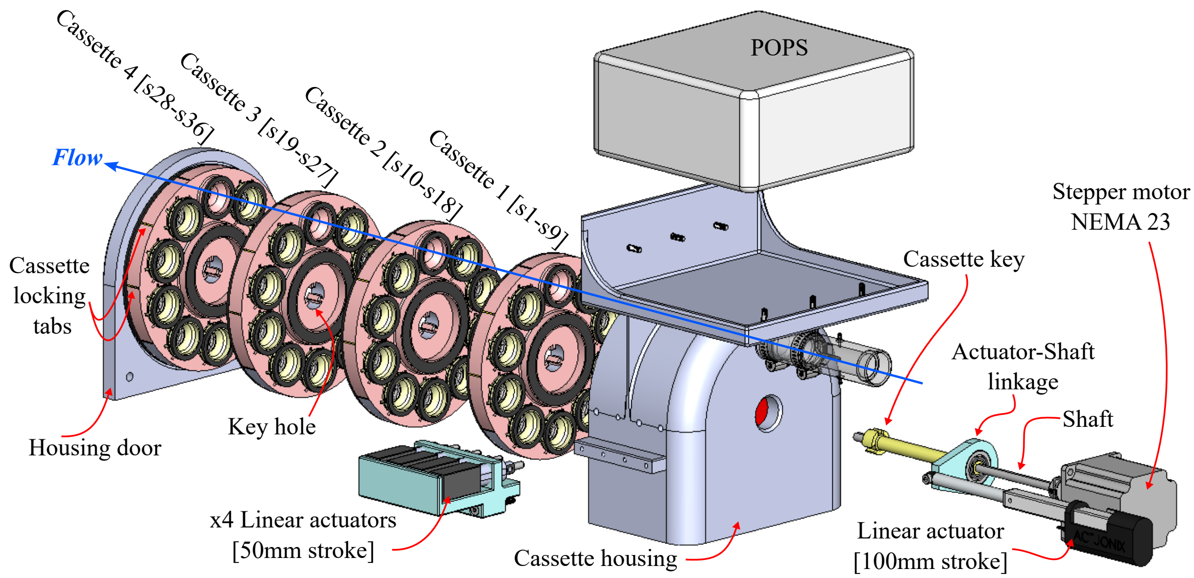

Figure 5: Schematic of HASP-GASP cassette housing and filter selection system.

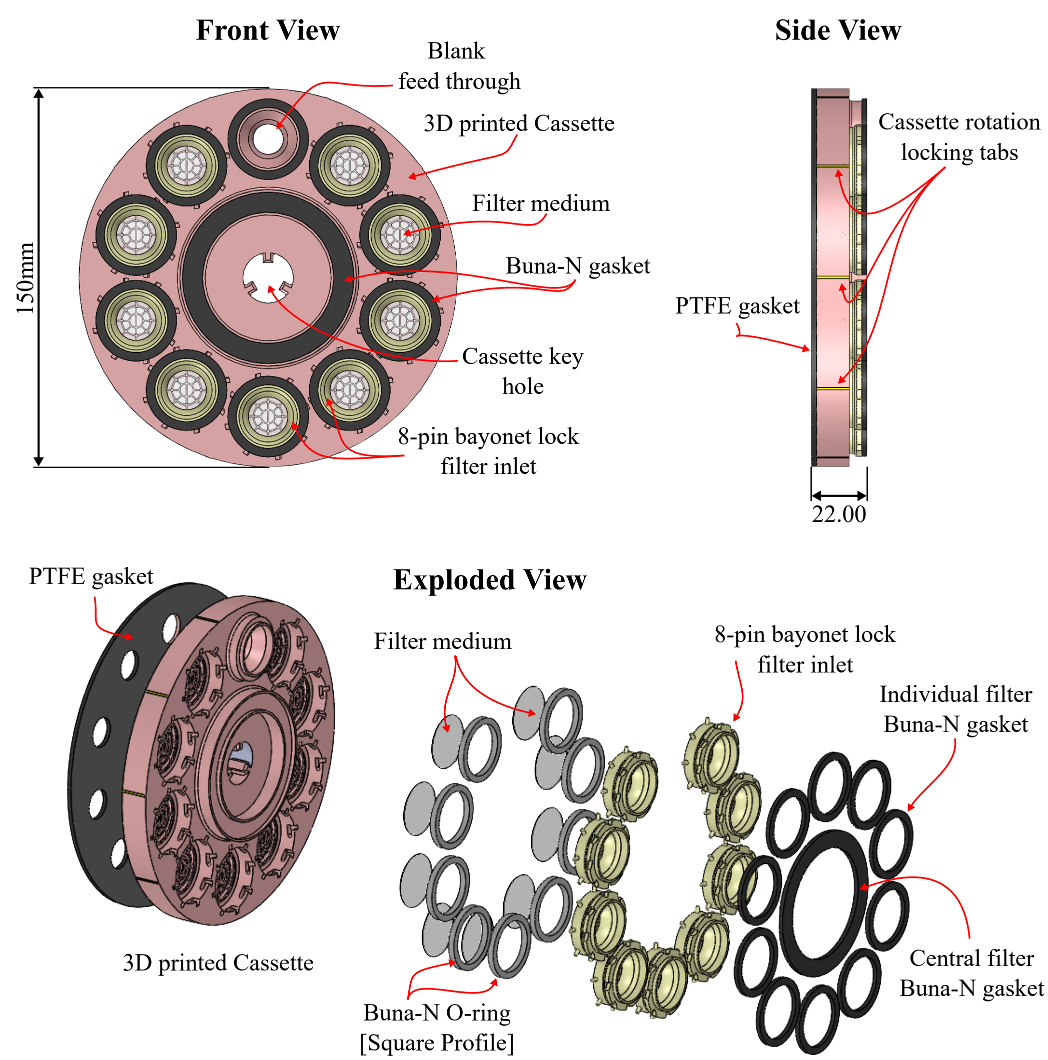

Figure 6: Schematic of HASP-GASP cassette assembly.

2.3.3 Portable Optical Particle Spectrometer (POPS)

The Portable Optical Particle Spectrometer (POPS), an off-the-shelf system from Handix Scientific, is designed to be a light-weight, high performance optical particle counter. It counts and measures the optical size of sampled particles using single-particle light scattering between approximately $140\mu m$ and $3\mu m$. For HASP 2022, a POPS-1100 model (also referred to as MPOS, Modular Optical Particle Spectrometer) will operate in isolation of the primary HASP-GASP science payload and will offer complementary *in-situ* data that can be tied back to aerosols collected on specific filter mediums. The POPS system was originally developed by the Chemical Sciences Division of the US National Oceanic and Atmospheric Administration (NOAA) and is licensed to Handix Scientific LLC. Contributions of the POPS system to the mass and power budget are included in Sections 3.1 and 3.2, respectively.

The POPS unit is a Class 1 Laser product. The optical chamber consists of the main sampling enclosure, which houses the laser diode, focusing optics, light collection mirror, laser beam dump, photo detector and inlet and exhaust ports. The laser beam produced by a $70mW$, $405nm$ laser diode is aligned to the horizontal center of the optical chamber, shown in Figure 7. Information regarding the Laser contained in the POPS unit is limited and personal communications with Handix Scientific is ongoing. Available information is provided in Appendix **D.**

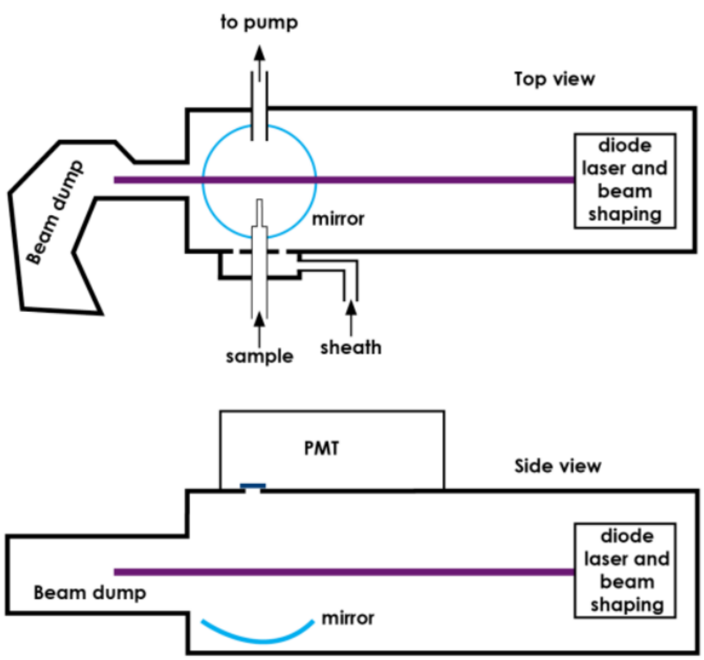

Figure 7: Schematic showing top and side views of the POPS Optical particle detection chamber and main components. Figure adapted from POPS user manual.

2.4 Mechanical Design

The primary structure of the HASP-GASP payload is composed of seven vertically mounted, and six horizontally mounted, 6560 Aluminium T-slot rails (Temper rating: T6). These T-rails are connected via M5 bolts to 6061 Aluminium L-brackets which are mounted to $3mm$ thick 6061 Aluminum base and roof plates. The base plate is mounted to the PVC HASP mounting plate via 27 M4 countersunk bolts, as indicated in Figure 16, Appendix **B**.

Figure 8 illustrates the mechanical layout of the HASP-GASP payload, with structural and non-structural components separated. The cassette housing is mounted to a secondary internal PVC plate. The AMETEK pump mounting system, the cassettes, cassette housing, power box, and electrical box will be custom designed and 3D printed on a FormLabs, Form2, stereolithography desktop 3D printer. The

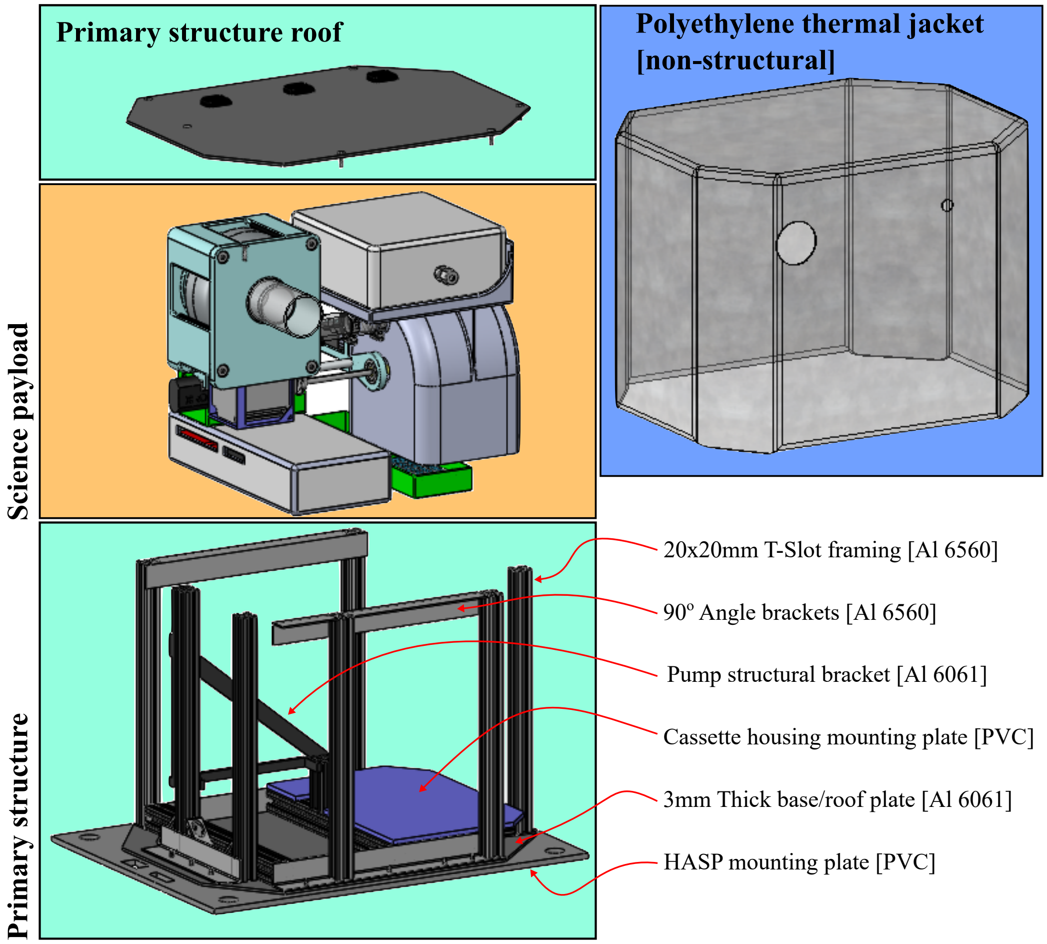

Figure 8: Payload structural layout.

HASP team has two of these at our disposal. These components will be printed from methacrylate photopolymer resin, resulting in components having a matte white finish and a density of $2g/cm^3$, printed to a resolution of 50 microns. Components for UMD payloads have been shown to have good reliability, low heat deformation, little cold embrittlement, and good impact strength, when printed with this material. Solid components typically demonstrate: ultimate tensile strength of $65MPa$; tensile modulus of $2.8GPa$; and flexural modulus of $2.2GPa$.

2.5 Electrical Design

A preliminary electrical schematic is provided in Figure 9. Power requirements for the various modes of operation are discussed in Section 3.2.

Under nominal conditions HASP power will be used to power the POPS unit, the primary and secondary computer systems and sensors (Arduino Mega 2560 based systems), the AMETEK centrifugal blower (at altitudes $> 24km$), and the filter selection subsystem composed of five linear actuators and a stepper motor with driver. For low altitudes (those $< 24km$), on board 16 Tenergy 18650 Li-ion cells (providing $40V_{dc}$ and $10,400mAh$) will be used to obtain aerosol samples. This is done as power requirements to achieve this will exceed the $2.5A$ limit provided from HASP power at $30V_{dc}$. Six samples below $24km$ will be acquired: one on the ground, and five during ascent. Switching between internal battery power and HASP power will be controlled via mechanical latching relays $R1$ and $R2$. Current protection systems will trigger $R1$ to open if $2.45A$ current draw is exceeded. This will protect HASP-GASP from blowing a fuse on the main gondola. Internal battery power will not be used by the pump if $R2$ is closed. Note, $R1$ and $R2$ will have

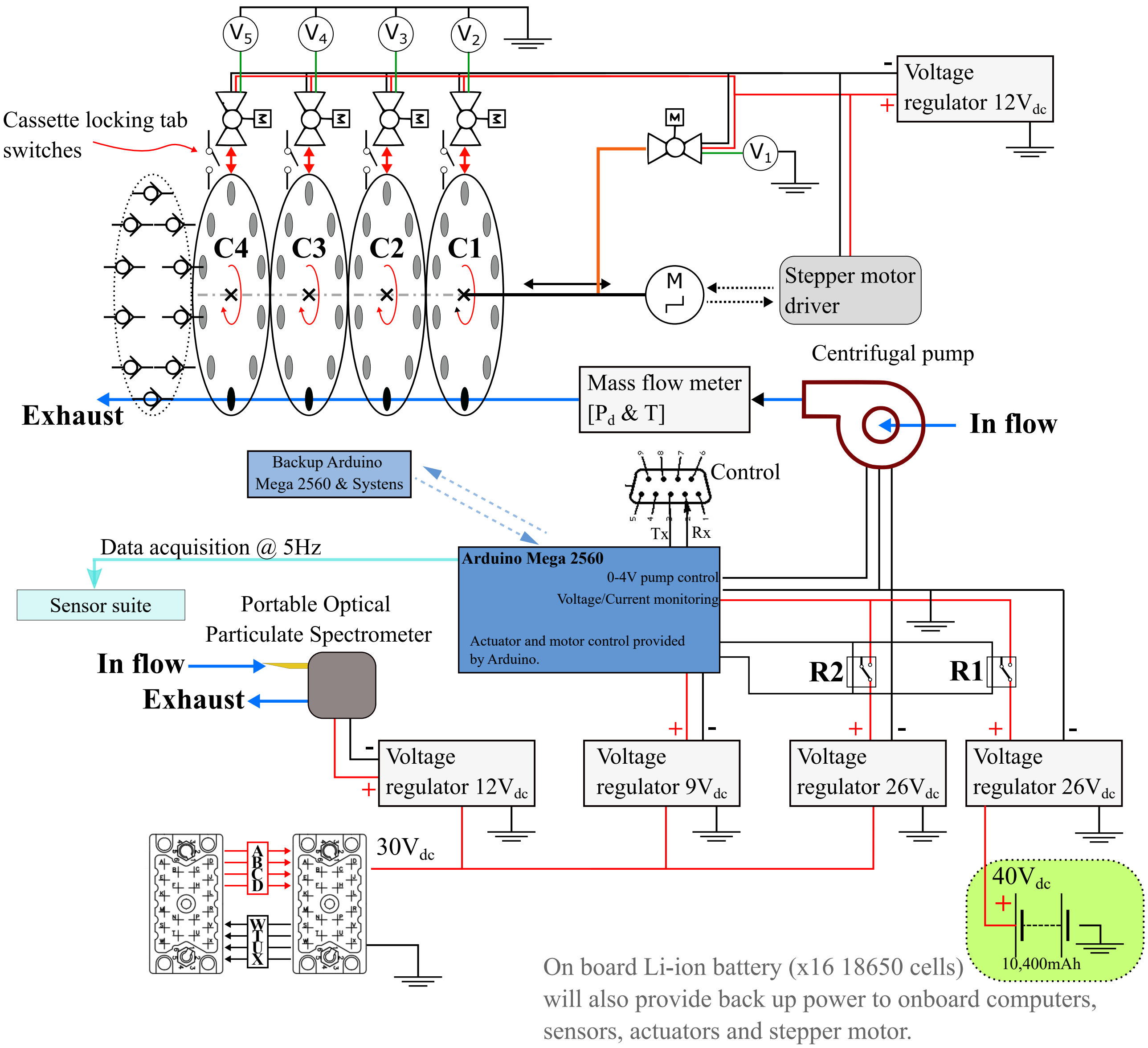

Figure 9: Preliminary electrical schematic of HASP-GASP systems.

robust criteria to ensure that they can not be closed at the same time. Failure modes of these relays will also be such that they fail open - back-up relays will be built in for potential payload recovery.

Switching from internal Li-ion batteries to HASP power will have to meet strict requirements. Two independent GPS signals, and three pressure sensors will be cross checked to ensure that the centrifugal blower cannot utilize HASP power unless the payload is $> 24km$.

Thirty-six (36) filter samples will be stored across four cassettes (**C1**, **C2**, **C3**, and **C4**). Actuator position V_1 will be used to drive the cassette key into the appropriate cassette lock. When engaged, monitored by V_1 the actuator will lock. If engaged with cassette **C3**, for example, linear actuator V_3 will disengage **C3**'s rotation locking tab (see Figure 6), so that it is free to rotate. The stepper motor will then rotate to align the appropriate filter medium (driver enables rotations accurate to 0.8°). Once aligned, linear actuator V_3 will engage **C3**'s rotation locking tab. Note, each rotation locking tab (of which there are ten per cassette, with separation of 36°) will be linked to internal potentiometers (inside the cassette). Thus, upon rotation of a cassette: 1) actuator V_1 will confirm engagement with the appropriate cassette; 2) actuators V_2, V_3, V_4, and V_5 will firstly confirm if the respective cassettes are rotationally locked or free to move, while cassette internal voltage dividers will indicate the filter is aligned with the mass flow meter;

and 3) the angle of the cassette mated to the stepper motor (known via V_1) is known via the stepper motor driver.

2.6 Thermal Control

As with UMD-HASP payloads in 2017, 2018, and 2019, HASP-GASP will not have active thermal management. The thermal jacket lining of the payload, expanded polyethylene foam, will offer a robust insulative barrier as determined from 25 sounding balloon flights and on UMD's HASP 2019 payload, HAAT. Based on the quantitative performance and experience gained in previous payload flights, this configuration is expected to keep HASP-GASP within an acceptable temperature range. The external side of the jacket will be white to minimize absorption of IR, while the interior side of the jacket will be highly reflective to help maintain internal heat. The expected performance/stability of HASP-GASP's internal temperature will also be verified by test. The entire HASP-GASP system will undergo at least one thermal test, and possibly one vacuum test, in the UMD thermal and vacuum chambers to verify payload operation down to $-60°C$ and $100Pa$, respectively, for a period of 6-7 hours. Additionally, all sensors and electronics in the 2022 HASP payload will also be flown at least six times on board *wee*-GASP via high altitude sounding balloons [*wee*-GASP operates with a nominal internal temperature of $+50°C$, which is passively maintained by dumping the heat from the AMETEK blower into the payload]. Lastly, HASP-GASP will also be tested in the thermal-vacuum test at CSBF during HASP integration in Palestine, TX.

The thermal chamber at UMD can go to both high and low temperatures, but for the purposes of this project will be used to test the system to a temperature of $-60°C$. The chamber will be held at the target temperature for a minimum of 6 hours to cold soak the hardware. Subsequently, the thermal chamber will subject HASP-GASP to $+60°C$ to test overheat protection systems. If HASP-GASP overheats, the pump will go into low power *ventilation* mode (MODE 10) to try to bring the internal temperature down. If the internal temperature exceeds $+80°C$, HASP-GASP will revert to power Mode 1 (Table 3 in Section 3.2) in order to cool down. On completion, the chamber will be brought back to room temperature, and the data logs will be examined to ensure that all equipment remained functional. If necessary, this testing can be iterated along with hardware modifications until all systems function reliably for the entire duration of the test.

The vacuum chamber can achieve pressures similar to those at $35km$. It does not have thermal controls, but may be used to identify potential issues with the electronics (*i.e.* arcing), which will be monitored for the duration of the testing.

HASP-GASP's electronics and sensors will also be tested on a minimum of six sounding balloon flights prior to CSBF integration. Three of these flights will typically last 1.5 to 2 hours and reach a maximum altitude between 24 and $35km$. The other three will coincide with the development of a tandem sounding balloon flight train designed to enable *wee*-GASP to either float or descend slowly ($< 2m/s$). These flights are planned to last 5 to 7 hours and reach a maximum altitude between 24 and $35km$ also. Though these flights may not last long enough to cold soak the payload, it will provide a baseline assessment of flight readiness.

The closest simulation that can be achieved pre-flight will be the thermal-vacuum test at CSBF. All systems are expected to work during this test, but if they do not there are strategies that can be implemented to address the issue. If the electronics get too cold, additional insulation and/or resistive heating would be added. Conversely, if the electronics get too warm heat-sinks can be added and/or increased in size and utilized to remove heat from the payload or specific payload components.

3 Payload Interface Specifications

3.1 Payload Mass Budget

A mass breakdown of HASP-GASP components is provided in Table 2. Individual component mass uncertainty is determined via systematic measurement error, prediction error (variable), or a standard error of $\pm 10g$ is assumed if the item's mass has been taken from respective specification sheets. From Table 2 it is anticipated that the HASP-GASP payload will be $1537g$ under the mass budget for a large payload. The mass of components is well understood with manageable uncertainty.

3.2 Payload Power Budget

The payload will use the EDAC 516-020 connector to provide power to the data acquisition system, computers, sensors (thermocouples, pressure sensors, etc.), POPS unit, AMETEK blower, stepper motor and drive, and P16 actuators (all five) as indicated previously in figure 9. Voltage will be regulated, actively monitored, and distributed according to each sub-system's power requirements. The power specifications of the payload remain within the limits of $+30V_{dc}$ at $2.5A$ (75 Watts) for the large payload classification at all times.

There are 5 primary modes that HASP-GASP will operate in during nominal operation, with an additional two modes discussed here. There are a total of 15 possible power modes - only the most power intensive arrangements are shown. The additional 8 modes of operation not discussed here are various potential settings to accommodate/navigate sub-system failures, all demanding lower power relative to the primary 5 modes.

The primary five power modes of operation are discussed below. Additional modes 6 and 7 are failure modes that could arise.

- **MODE 1**: HASP-GASP is on and actively monitoring payload health and ambient conditions. Pump, POPS unit, and filter selection sub-system (actuators and stepper motor) are off. Power budget summary provided in Table 3.
- **MODE 2**: HASP-GASP is on and actively monitoring payload health and ambient conditions, POPS Unit is on and acquiring data. Pump and filter selection sub-system (actuators and Stepper motor) are off. Power budget summary provided in Table 4.
- **MODE 3**: HASP-GASP is on and actively monitoring payload health and ambient conditions, POPS Unit is on and acquiring data. Filter selection sub-system (actuators and stepper motor) are on. This mode is used to select the subsequent sample filter (a total of 36 samples) located on one of four cassettes. Power budget summary provided in Table 5.
- **MODE 4**: HASP-GASP is on and actively monitoring payload health and ambient conditions with POPS unit on. Filter selection sub-system is locked into place. The centrifugal AMETAK blower is disconnected from HASP power and connected to the internal Li-ion batteries. This configuration is used to collect samples at altitudes $< 24km$. Assumed operation point, shown in Table 6, is at sea level - i.e. most power demanding scenario possible.
- **MODE 5**: This signifies nominal operations at altitudes $> 24km$. All systems are running and pump is transporting mass flow through a filter. Table 7 and Table 8 show power demand at $24km$ [$\approx 27mbar$] (highest power demand condition from HASP) and $35km$ [$\approx 8mbar$] (nominal power demand at float), respectively.

Item	Supplier	Mass (g)	Qnty	Total Mass (g)	Uncertainty (g)	Source
POPS Unit	Handix	600.0	1	600.0	±10	Spec.
Li-ion Batteries	Tenergy	374.0	2	748.0	±0.1	Meas.
Blower	AMETEK	541.0	1	541.0	±0.1	Meas.
P16 Actuator [100mm]	Actuonix	110.0	1	110.0	±10	Spec.
P16 Actuator [50mm]	Actuonix	95.0	4	380.0	±10	Spec.
Stepper Motor	McMaster	681.8	1	681.8	±0.1	Meas.
Al 6560 T-slot Ext.	McMaster	139.7	13	1816.1	±0.1	Meas.
Al 6560 90^o brackets	McMaster	14.7	3	44.1	±0.1	Meas.
Al 6061 L-brackets	McMaster	66.5	4	266	±50	Pred.
Double-loop coupling	McMaster	153.0	1	153.0	±10	Spec.
Bearings	McMaster	47.7	2	95.4	±10	Spec.
1/4" Shaft	McMaster	236.9	1	236.9	±50	Pred.
Pump Heat-sink	McMaster	32.8	1	32.7	±50	Pred.
PVC mounting plate	McMaster	405.7	1	405.7	±50	Pred.
Check-valve	McMaster	12.0	10	120.0	±0.1	Meas.
O-rings	McMaster	2.3	36	82.8	±0.1	Meas.
BUNA-N Gasket	McMaster	164.0	1	164.0	±50	Pred.
PTFE Gasket	McMaster	123.0	1	123.0	±50	Pred.
Fasteners	McMaster	270.0	1	270.0	±100	Pred.
Comp. + Sens.	Various	374.0	1	374.0	±50	Meas.
Voltage Regs.	Various	90.7	4	362.8	±0.1	Meas.
GPS antenna	Adafruit	54.4	3	163.2	±0.1	Meas.
Wiring	Various	800.0	1	800.0	±100	Pred.
Al Roof plate	Inhouse	893.5	1	893.5	±50	Pred.
Al Base plate	Inhouse	892.7	1	892.7	±50	Pred.
Al Brackets	Inhouse	254.8	1	254.8	±50	Pred.
Motor Bracket	Inhouse	168.0	1	168.0	±0.1	Meas.
Pump housing	Inhouse	1374.2	1	1374.2	±100	Pred.
Elec. Boxs	Inhouse	524.7	1	524.5	±100	Pred.
Power box	Inhouse	1060.9	1	1060.9	±100	Pred.
Act. Link	Inhouse	20.3	1	20.3	±0.1	Meas.
Cassette Key	Inhouse	15.8	1	15.8	±0.1	Meas.
Actuator support	Inhouse	224.9	1	224.9	±0.1	Meas.
Cassette housing	Inhouse	2984.2	1	2984.2	±100	Pred.
Cassette	Inhouse	146.5	4	586.0	±100	Pred.
Inlet	Inhouse	9.2	36	331.2	±50	Pred.
Flow meter	Inhouse	15.2	1	15.2	±50	Pred.
Thermal Jacket	Inhouse	554.2	1	554.2	±100	Pred.
Total				18,462.1	±1401.4	

Table 2: Payload mass summary.

- **MODE 6**: Operations at altitudes $> 24km$, with the primary computer, Comp 1, failing and the secondary computer, Comp 2, brought entirely online. All systems are running and pump is transporting mass flow through a filter. Table 9 shows power demand at $35km$ [$\approx 8mbar$] (contingency power demand at float).

- **MODE 7**: In Mode 7, HASP-GASP has lost power from HASP. The purpose of Mode 7 is to quickly secure all filter samples into place in an emergency. Cassettes will be locked into their safe condition in < 60 seconds, and will subsequently power down. Power budget summary provided in Table 10.

When assessing the power budget summaries for the modes shown here, note that a current draw marked with an asterisk [*] has been assessed, monitored, and measured at UMD by the GASP team. For current draws that are not marked, and therefore not directly measured, current draw projections have been taken from part specification sheets or calculated using the specification sheet. All numbers are traceable and justified.

MODE 1

Item	**Average Current (mA) at 30 V**	**Peak Current (mA) at 30 V**	**Power Source**
Comp 1	0	0	Internal
Comp 2	0	0	Internal
POPS Unit	0	0	Internal
AMETEK Blower	0	0	Internal
Stepper Motor & Driver	0	0	Internal
P16 Actuator [100mm]	0	0	Internal
P16 Actuator [50mm]	0	0	Internal
Total Internal	**0 mA**	**0 mA**	
Comp 1	155*	155*	HASP
Comp 2	60*	155*	HASP
POPS Unit	0	0	HASP
AMETEK Blower	0	0	HASP
Stepper Motor & Driver	0	0	HASP
P16 Actuator [100mm]	0	0	HASP
P16 Actuator [50mm]	0	0	HASP
Total (from HASP)	**215 mA**	**310 mA**	

Table 3: **Mode 1** power budget summary.

MODE 2

Item	Average Current (mA) at 30 V	Peak Current (mA) at 30 V	Power Source
Comp 1	0	0	Internal
Comp 2	0	0	Internal
POPS Unit	0	0	Internal
AMETEK Blower	0	0	Internal
Stepper Motor & Driver	0	0	Internal
P16 Actuator [100mm]	0	0	Internal
P16 Actuator [50mm]	0	0	Internal
Total Internal	**0 mA**	**0 mA**	
Comp 1	155*	155*	HASP
Comp 2	60*	155*	HASP
POPS Unit	416	416	HASP
AMETEK Blower	0	0	HASP
Stepper Motor & Driver	0	0	HASP
P16 Actuator [100mm]	0	0	HASP
P16 Actuator [50mm]	0	0	HASP
Total (from HASP)	**631 mA**	**726 mA**	

Table 4: **Mode 2** power budget summary.

MODE 3

Item	Average Current (mA) at 30 V	Peak Current (mA) at 30 V	Power Source
Comp 1	0	0	Internal
Comp 2	0	0	Internal
AMETEK Blower	0	0	Internal
Stepper Motor & Driver	0	0	Internal
P16 Actuator [100mm]	0	0	Internal
P16 Actuator [50mm]	0	0	Internal
Total Internal	**0 mA**	**0 mA**	
Comp 1	155*	155*	HASP
Comp 2	60*	155*	HASP
POPS Unit	416	416	HASP
AMETEK Blower	0	0	HASP
Stepper Motor & Driver	650*	886*	HASP
P16 Actuator [100mm]	80	100	HASP
P16 Actuator [50mm]	80	100	HASP
Total (from HASP)	**1441 mA**	**1812 mA**	

Table 5: **Mode 3** power budget summary.

MODE 4

Item	Average Current (mA) at 30 V	Peak Current (mA) at 30 V	Power Source
Comp 1	0	0	Internal
Comp 2	0	0	Internal
AMETEK Blower	3356*	6000*	Internal
Stepper Motor & Driver	0	0	Internal
P16 Actuator [100mm]	0	0	Internal
P16 Actuator [50mm]	0	0	Internal
Total Internal	**3356 mA**	**6000 mA**	
Comp 1	155*	155*	HASP
Comp 2	60*	155*	HASP
POPS Unit	416	416	HASP
AMETEK Blower	0	0	HASP
Stepper Motor & Driver	100*	120*	HASP
P16 Actuator [100mm]	8	100	HASP
P16 Actuator [50mm]	8	100	HASP
Total (from HASP)	**747 mA**	**1046 mA**	

Table 6: **Mode 4** power budget summary.

MODE 5 @ $24km$

Item	Average Current (mA) at 30 V	Peak Current (mA) at 30 V	Power Source
Comp 1	0	0	Internal
Comp 2	0	0	Internal
AMETEK Blower	0	0	Internal
Stepper Motor & Driver	0	0	Internal
P16 Actuator [100mm]	0	0	Internal
P16 Actuator [50mm]	0	0	Internal
Total Internal	**0 mA**	**0 mA**	
Comp 1	155*	155*	HASP
Comp 2	60*	155*	HASP
POPS Unit	416	416	HASP
AMETEK Blower	728*	1356*	HASP
Stepper Motor & Driver	100*	120*	HASP
P16 Actuator [100mm]	8	100	HASP
P16 Actuator [50mm]	8	100	HASP
Total (from HASP)	**1475 mA**	**2402 mA**	

Table 7: **Mode 5** power budget summary under nominal operation at $24km$ [$27mbar$].

MODE 5 @ 35km

Item	**Average Current (mA) at 30 V**	**Peak Current (mA) at 30 V**	**Power Source**
Comp 1	0	0	Internal
Comp 2	0	0	Internal
AMETEK Blower	0	0	Internal
Stepper Motor & Driver	0	0	Internal
P16 Actuator [100mm]	0	0	Internal
P16 Actuator [50mm]	0	0	Internal
Total Internal	**0 mA**	**0 mA**	
Comp 1	155*	155*	HASP
Comp 2	60*	155*	HASP
POPS Unit	416	416	HASP
AMETEK Blower	562*	1356*	HASP
Stepper Motor & Driver	100*	120*	HASP
P16 Actuator [100mm]	8	100	HASP
P16 Actuator [50mm]	8	100	HASP
Total (from HASP)	**1309 mA**	**2402 mA**	

Table 8: **Mode 5** power budget summary under nominal operation at 35km [8$mbar$].

MODE 6 @ 35km

Item	**Average Current (mA) at 30 V**	**Peak Current (mA) at 30 V**	**Power Source**
Comp 1	0	0	Internal
Comp 2	0	0	Internal
AMETEK Blower	0	0	Internal
Stepper Motor & Driver	0	0	Internal
P16 Actuator [100mm]	0	0	Internal
P16 Actuator [50mm]	0	0	Internal
Total Internal	**0 mA**	**0 mA**	
Comp 1	0	0	HASP
Comp 2	155*	155*	HASP
POPS Unit	416	416	HASP
AMETEK Blower	562*	1356*	HASP
Stepper Motor & Driver	100*	120*	HASP
P16 Actuator [100mm]	8	100	HASP
P16 Actuator [50mm]	8	100	HASP
Total (from HASP)	**1249 mA**	**2247 mA**	

Table 9: **Mode 6** Power budget summary at 35km [8$mbar$] with computer 1 off.

MODE 7

Item	Average Current (mA) at 30 V	Peak Current (mA) at 30 V	Power Source
Comp 1	155*	155*	Internal
Comp 2	60*	155*	Internal
AMETEK Blower	0	0	Internal
Stepper Motor & Driver	650*	886*	Internal
P16 Actuator [100mm]	80	100	Internal
P16 Actuator [50mm]	80	100	Internal
Total Internal	**1025 mA**	**1396 mA**	
Comp 1	0	0	HASP
Comp 2	0	0	HASP
POPS Unit	0	0	HASP
AMETEK Blower	0	0	HASP
Stepper Motor & Driver	0	0	HASP
P16 Actuator [100mm]	0	0	HASP
P16 Actuator [50mm]	0	0	HASP
Total (from HASP)	**0 mA**	**0 mA**	

Table 10: **Mode 7** Power budget summary for sample-safeing operation.

3.3 Downlink Serial Data

Communication will be achieved with the HASP gondola over a RS232 shifter, as Arduino does not have a built-in RS232 output. This RS232 shifter will take the TTL output from the Arduino and manipulate it to RS232 levels, facilitating communication. Arduino's native TTL Serial library can then be throttled to a 4800 baud rate, which should guarantee that HASP-GASP will not exceed the allotted bandwidth. Table 11 presents an example data packet structure of 520 bytes.

Title	Byte	Description
Header	1-2	Indicates start of new data packet
Origin	3	I2C ID specific to the system that generated the data
Time send gondola	4-12	8-byte time sent from gondola
Time send origin	13-21	8-byte time sent from origin system
No. of data blocks	22	No. of different data blocks in data packet
Total size of data blocks	23-24	Two-bytes: total size of data packet
Checksum	25-30	Checksum
Data Packet	31-518	Payload and ambient conditions
Terminate	519-520	Indicates end of packet

Table 11: Serial downlink, assuming data packet of 520 Bytes.

3.4 Uplink Serial Commanding

Large payloads on HASP are able to send commands from the ground at a baud rate of 4800. This Serial Uplink system allows for payloads to be instructed via the HASP gondola over an RS232 line; the HASP gondola then communicates with the ground station.

Table 12 presents the anticipated command List; Byte1: I2C ID [0x00] and Byte2: Command ID.

Name	Command ID	**Function**
Computer rests	0x52	Arduino/sensor reset
System rests	0x53	Full hard reset of Payload
POPS rests	0x54	POPS power cycle
Run diagnostics	0x44	System health check
Arm Pump	0x41	Connected to power but not running
Idle Pump	0x49	Connected to power and idling
Ping	0x50	Payload Status
Manual Sample selection	TBD	Select individual sample
Full Stop	0x60	Stop pumps [Open relay]
Pause Stop	0x61	Momentarily pause pumps
Reset current protection system	0x38	Reset R2
Mode1	0x31	Set to power Mode 1
Mode2	0x32	Set to power Mode 2
Mode3	0x33	Set to power Mode 3
Mode4	0x34	Set to power Mode 4
Mode5	0x35	Set to power Mode 5
Mode6	0x36	Set to power Mode 6
Mode7	0x37	Set to power Mode 7
Safe stop and shut down	0x66	Isolate samples, prepare for descent

Table 12: Serial command list.

3.5 Payload Location and Orientation

All of the experimental goals are independent of the physical location on the HASP gondola. However, the stern side of the gondola is deemed to be best suited for GASP as it is farthest from the launch vehicle prior to launch [30], thus favoring either payload locations 09 or 10 as indicated in Figure 10. The HASP-GASP payload will be orientated with flow intakes pointing away from the main gondola (orientation shown in Figure 10), and will not reach out beyond the ground footprint of the mounting base-plate. Necessary modifications to the HASP mounting plate are shown in Figure 16 (Appendix B).

3.6 Special Requests

The University of Maryland team has no special requests for HASP-GASP.

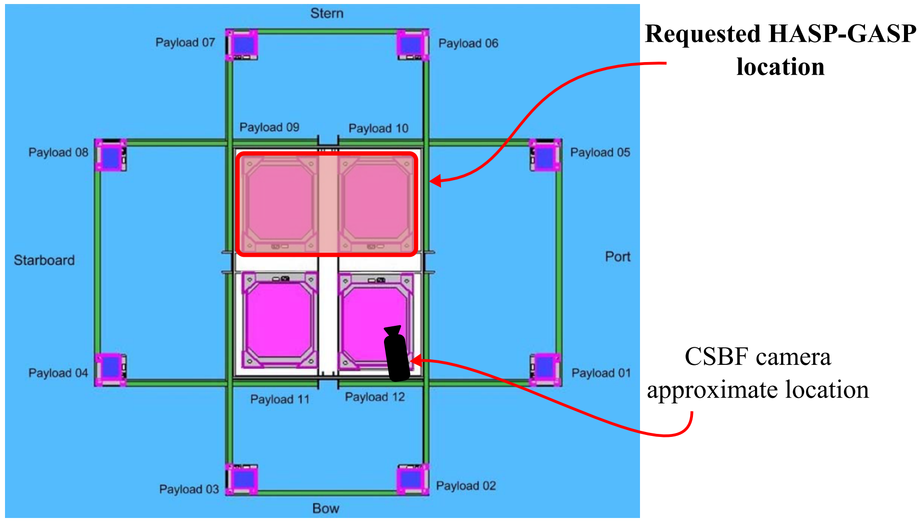

Figure 10: Requested payload location on the stern of the HASP gondola. View is top down.

4 Payload Summary

In summary, the HASP-GASP (HASP 2022) payload is a large class payload that will measure local atmospheric conditions while collecting 36 aerosol samples each acquired from $1.225kg$ ($1m^3$ of air at standard temperature and pressure) of processed air at altitudes between $< 1km$ to $36km$. Data will be recorded onto a robust data acquisition system with non-volatile flash memory. A summary of the HASP-GASP payload is shown in table 13.

Item	Units
Total Mass	$18,462g$
Average Current Draw from HASP at $35km$ float	$1309mA$
Peak Current Draw from HASP at $35km$ float	$2402mA$
Payload Size	Large
Payload Footprint	$402 \times 315mm$
Payload Height	$300mm$ above mounting plate
Payload Location	Stern side of gondola; locations 09 or 10
Payload Orientation	Intakes pointed away from HASP Pallet
Discrete Commands	DAS On/Off (F, N)
Downlink serial data	4800 baud payload status
Uplink serial commands	Yes
Analog Downlink	None

Table 13: HASP-GASP payload summary.

Detailed mass and power budgets can be found in Sections 3.1, and 3.2, respectively.

5 Project Management

5.1 Team Organization and Roles

There are four preliminarily student leads: 1) **Matthew Killian**, a first-year graduate student in the High-Speed Aerodynamics and Propulsion Lab (HAPL), will lead the payload instrumentation, aerosol collection system, and data analysis effort. **Matthew** will also provide oversight of all documentation and software necessary for this project. 2) Undergraduates **Saimah Siddiqui** and **Julianna Reese** will direct electronics design and integration of associated systems/software. 3) Undergraduate **Cameron Storey**, will be directing structural design and assembly of HASP-GASP. There are also four undergraduate subsystem leads: 1) **Jeremy Kuznetsov** who will take charge of mechanical subsystems; 2) **Alejandro Tovar** will take charge of thermal management and associated subsystems; 3) **Chaitanya Garg** who will take charge of sensor integration and software; and 4) **Andrew Simone** will take charge of mechanical subsystems and filter selection hardware. **Finnegan O'Neill** will support the team by leading computational analysis of the payload - specifically static thermal and structural (finite element) analysis.

An additional seven undergraduates will be assisting on the HASP project as well, operating as a support team for trouble shooting and aiding where required; see Table 16 in Appendix **A** for full team personnel, with the additional seven supporting undergraduates listed in Table 17. Contact information for key faculty and leadership personnel is highlighted in Table 18.

The UMD faculty advisors are **Dr. Mary Bowden** and **Dr. Stuart Laurence**, with **Dr. Shaun Skinner** serving as Project Manager and Science and Engineering Lead for the HASP-GASP payload. **Dr. Mary Bowden** is the director of the University of Maryland's Balloon Payload Program (sponsored by the Maryland Space Grant Consortium) and provides expert advice in balloon flight operations. **Dr. Stuart Laurence** is the lead PI for UMD's LDRD Exploratory Research [Proposal Title: High Altitude Disturbance: An Integrated Experimental and Modeling Approach to Quantifying Turbulence and Aerosols at Hypersonic Flight Height]. **Dr. Shaun Skinner** is a Post Doctoral researcher at UMD funded through the LDRD program. **Dr. Sonia Wharton**, **Dr. Alan Hidy**, and **Dr. Tom Ehrmann** will provide support and guidance from Lawrence Livermore National Laboratory (which is a federally funded research and development center [FDRCC]).

5.2 Timeline and Milestones

Table 14 outlines the major tasks to be completed from January 2022 to July 2022 to have HASP-GASP ready for CSBF integration and, subsequently, flight on the HASP gondola in early September. Planned FiSH and *wee*-GASP flights have been included in the timeline as *wee*-GASP and HASP-GASP will share sensors, electronics, and data acquisition systems. It is anticipated that between three and six undergraduate students will be available to participate in integration at CSBF, and between two and three students will participate in flight operations at Ft. Sumner, NM.

5.3 Anticipated Participation on Integration and Launch Operations

At this time, it is anticipated that **Matthew Killian**, **Saimah Siddiqui**, and **Julianna Reese**, led by **Dr. Shaun Skinner**, will attend both integration in Palestine, TX, and Flight Operations in Fort Sumner, NM.

6 Integration Procedures

Upon arrival at CSBF for HASP integration, HASP-GASP will be bolted to the top of the payload mounting plate. Once secure, the thermal jacket will be installed and intakes covered until testing is ready. Testing shall include check-out of all payload systems, diagnostics of the pump and filter selection systems, and verification that both serial and discrete communications are properly routed, coded, and working. Once systems are operating as planned the payload will be ready for nominal operations. Several power modes will also be tested to ensure that fault detection and diagnostic systems are working as intended. Upon arrival at Ft. Sumner for the HASP flight, similar testing verification will be performed to ensure the payload is functional before flight. This is outlined in Table 15.

Table 14: Description of work.

2022 Time-line	**Description of work**
January	Undergraduate Additional hardware acquisition
7^{th} January	- HASP application due
7^{th}-18^{th} January	- FiSH flights out of Kessler Atmospheric and Ecological Field Station, Purcell, OK. Particulate ground testing with *wee*-GASP
28^{th} January	- Announcement of HASP selection of student payloads
February-March	- Structure development
	- Circuit design and manufacture
	- Aerosol sub-system assembly and testing
	- Design refinement
	- Hardware tests
	- FiSH and *wee*-GASP sounding balloon flights out of Maryland
March-April	- Payload structure and thermal jacket manufacture
April	- FiSH and *wee*-GASP sounding balloon flights out of Maryland
29^{th} April	- Preliminary PSIP document due
June	- Complete integration of HASP-GASP payload and sensors.
	- Drop tests.
	- Thermal and vacuum tests.
	- Full sensor calibration.
	- 2nd Thermal and vacuum tests.
	- FiSH and *wee*-GASP sounding balloon flights in collaboration with NASA's DCOTSS ER-2 experiment in Salina, KS.
24^{th} June	- NASA On-site Security Clearance Document due
24^{th} June	- Final PSIP document due
$\approx 25^{th}$-29^{th} July	- Student payload integration at CSBF.
$\approx 29^{th}$ Aug- 2^{nd} Sept.	- HASP flight preparation.
$\approx 3^{rd}$ September	- Target flight ready.
$\approx 5^{nd}$ September	- Target launch date and flight operations.
$\approx 7^{th}$-11^{th} September	- Recovery, packing and return shipping.
November	- Post-flight calibration of sensors.
November	- FiSH flight.
$\approx 9^{th}$ December	- Final Flight / Science Report due.

7 Preliminary Flight Operations Plan

Table 15: Preliminary flight plan. *Each sample at $35km$ will take ≈ 20 minutes to acquire.

Time from launch	Event name
- 01:00:00	Turn on payload and run full payload diagnostics
- 00:30:00	Run full payload diagnostics
- 00:15:00	Acquire one ground aerosol sample
+ 00:00:00	Balloon launches
+ 00:30:00	Acquire six aerosol samples during ascent
+ 02:00:00	Balloon reaches float altitude
+ 02:10:00	Run full payload diagnostics
+ 02:15:00	Begin acquisition of 30 aerosol samples while at float
+ 12:30:00	Send command to secure filter samples and prepare filters for passive re-pressurization. Perform heat dump ahead of descent
+ 24:00:00	Flight ends

8 Previous Balloon Flights

8.1 HASP

8.1.1 2008 - 2009

On the 2008 and 2009 HASP flights, the UMD ABC payloads (University of Maryland Advanced Balloon Communications Experiments) tested various configurations of GPS antennas and radio downlink systems. These GPS antennas successfully communicated with a ground station throughout the flight in 2009.

8.1.2 2010 - 2012

HASP 2010 was the first flight of the UMD payload StratoPigeon, which was designed to acquire data for a few hours before being deliberately dropped from the HASP gondola. StratoPigeon received its drop command through a ground station telemetry network similar to that tested during the ABC experiments. The 2010 flight was a systems check operation to ensure full system functionality. The 2011 and 2012 flights both demonstrated successful drops, but only the 2011 drop module was successfully tracked and recovered.

8.1.3 2017

The UMD HASP 2017 payload was a spiritual successor to StratoPigeon dubbed HAAT-TRIC. This was a partnership between the Balloon Payload Program (BPP) and the High-speed Aerodynamics and Propulsion Lab (HAPL), both research labs in the Aerospace Engineering Department at UMD. BPP provided the data drop module while HAPL supplied the scientific instrumentation and data. HAAT used a constant voltage anemometer coupled with thin-film probes to measure perturbations in velocity and temperature within the upper stratosphere, while TRIC contained a Raspberry Pi for data logging that was to be dropped when commanded with a HASP discrete signal. Due to hardware difficulties before flight, the drop module was dropped on a 4 hour timer instead of using the discrete command lines, and there was no serial downlink of the payload status.

Spectral data from the hot and cold thin-film probes from three regions between the altitude of $107.7kft$ and $109kft$ are presented in figure 11. Data was sampled at $30kHz$ for over 7 hours. Both $-5/3$ and -7 decay trends are observed, though the signal drops into noise at around $20Hz$. No measurements of

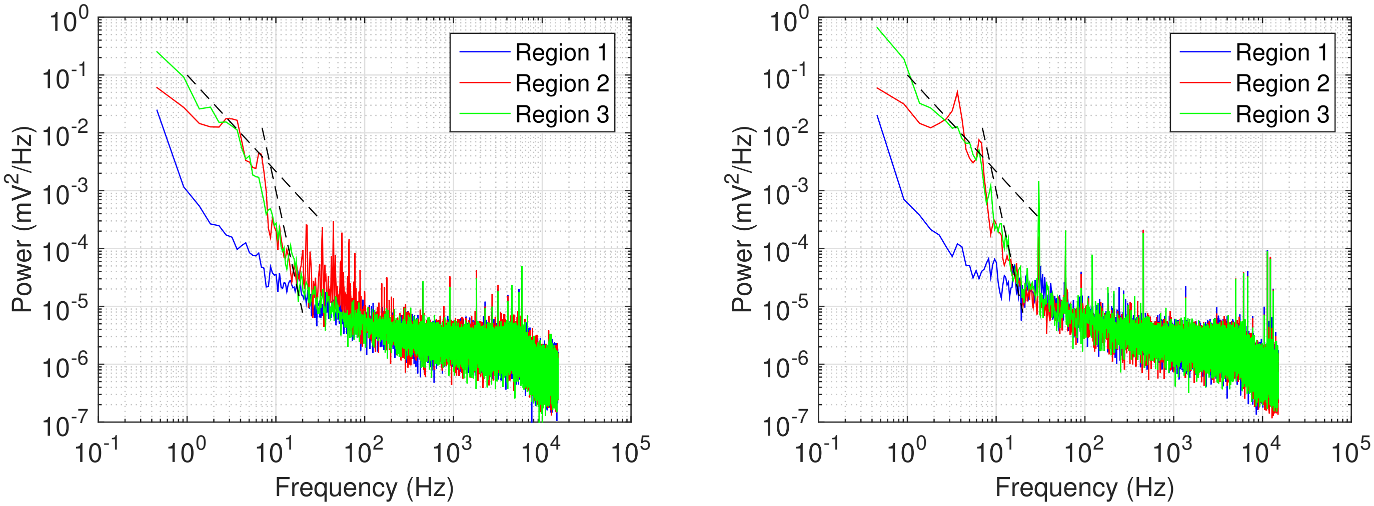

(a) Hot-film power spectra.

(b) Cold-film power spectra.

Figure 11: Data collected from thin-film probes on HASP 2017 flight; dashed lines indicate decays of $-5/3$ and -7.

the relative wind speed is available from HASP to derive length scales, hence the spectra is plotted in terms of frequency rather than wave number. This flight was a significant milestone in demonstrating the capabilities of our HAAT system for disturbance measurements over extended periods of time above $100kft$.

Although the HASP 2017 flight was successful in terms of data acquisition, HAAT-TRIC suffered structural failure on landing. The 3D printed structure that attached the payload to the HASP pallet was found to degrade under intense ultra-violate light and cold temperatures experienced at high altitude.

8.1.4 2018

In 2018, UMD flew the second iteration of the HAAT-TRIC payload on HASP. This payload was primarily focused on improving the previous year's design. However, the mini-CVA and film probes were replaced in HAAT, with a suite of microphones for the purpose of measuring high altitude acoustic fluctuations. Unfortunately, faulty connections prevented any microphone data from being recorded, although the payload proved fully operational during thermal vacuum testing at CSBF. TRIC functioned as planned with a tethered drop of the data module.

8.1.5 2019

For HASP 2019, UMD developed a new iteration of HAAT that combined the microphone and hot wire capabilities of the prior two flights. HAAT operated as intended, successfully acquiring 5:19 hours of data at 40kHz during the CSBF float. In flight, HAAT acquired data for 68% of the total mission time of 7 hours and 37 minutes (7:62 hours), and functioned as intended for the whole flight.

Acoustic interference from nearby payloads, while troublesome in nature, did serve to demonstrate the high sensitivity of HAAT's acoustic measurements at high altitudes. The main payloads which produced audible noise are shown in Figure 12. Of the full 5:19 hours of acquired data, there was only 115 seconds of data which was not contaminated by non-atmospheric noise. An additional 50 seconds of data was partially contaminated. Unfortunately, over these 165 seconds (spaced over three events of duration 50, 10, and 105 seconds) there are no distinct atmospheric pressure fluctuations; the noise floor of the 378A04 microphones was $\pm 0.004 Pa$.

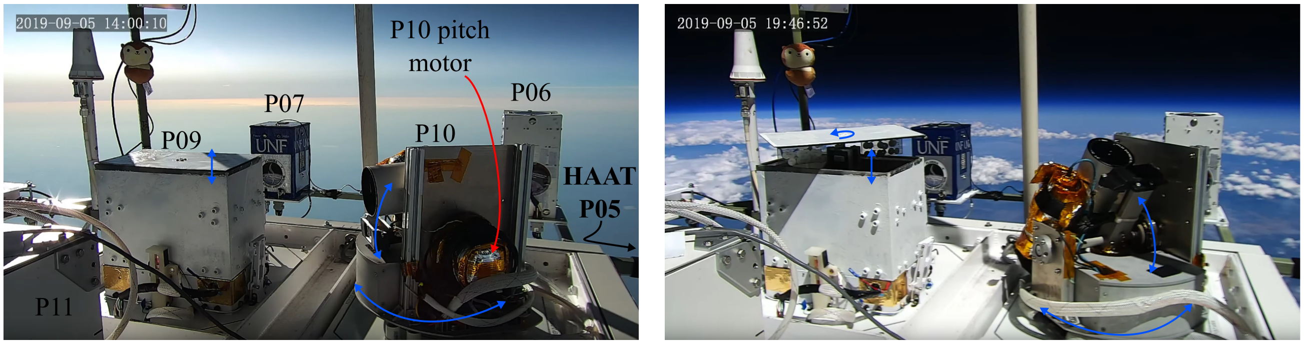

Figure 12: View from HASP 2019 CSBF camera indicating several payload locations relative to HAAT; note that the real time is shown in the top left of each frame. The blue line indicate the motions (controlled by stepper motors) for Payloads P09 and P10, which were positioned directly behind HAAT (P05).

In order to attempt to separate acoustic interference from possible atmospheric pressure fluctuations, we have to fully understand, to the best of our ability, noise from non-atmospheric sources. This is especially true for P10 as it is persistent and dominates all other pressure fluctuations. A little under half way through the CSBF float, at ≈19:00:00, provides the quietest period of time in terms of atmospheric pressure fluctuations. At this time only pressure fluctuations caused by P10 acoustics are observed. Figure 13 presents particularly clean acoustic signals detected by both microphones from P10 over a 10 seconds starting at 19:00:00. It is emphasized that this interference pattern from P10 is observed in 99.4% of all pressure fluctuation data recorded by HAAT. Through private communications, P10 is understood to have identical drives for pitch and yaw, hence it is not clear if these will produce differing acoustic signatures. Pressure fluctuation data demonstrates sharp peaks occurring at approximately $1.6s$ intervals ($\approx 0.625Hz$),

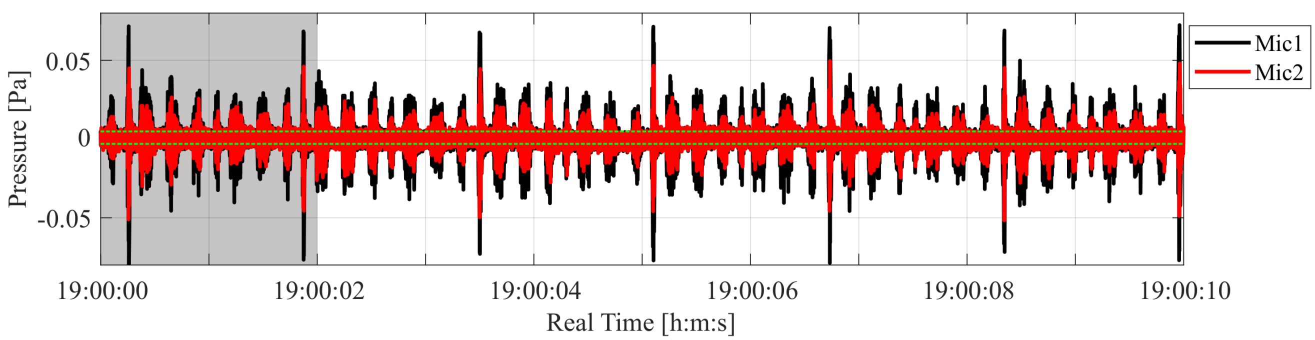

(a)

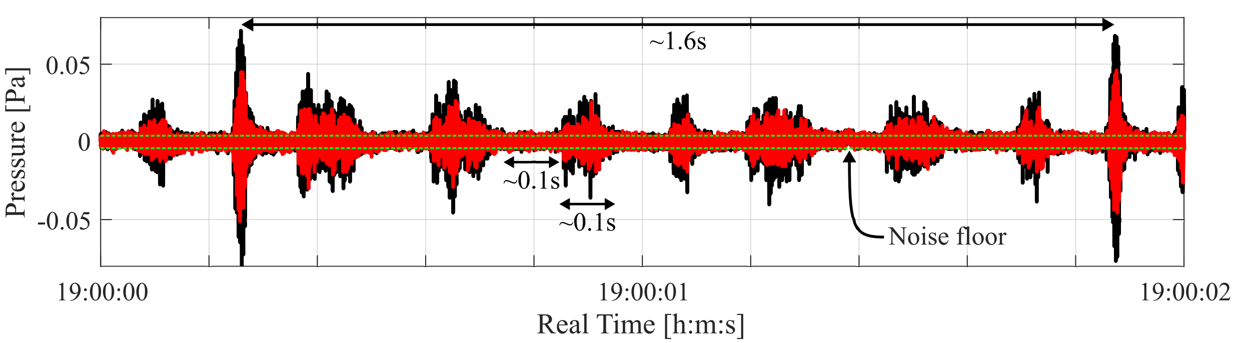

(b)

Figure 13: Pressure fluctuations detected by microphones 1 and 2 over a 10 second period at 19:00:00. This period of time has particularly low background noise, producing a very clean acoustic signal coming from P10.

in between which seven smaller/softer pulses with the same spectral content are observed. The frequency content is not observed to change, only the amplitude of the signal. Each of the pressure pulses observed are bounded by periods of quiet, and occur at frequency of $\approx 5Hz$. Unfortunately the frequencies produced by the neighboring payloads cannot be simply filtered out of the pressure fluctuation data. The reason for this is they coincide with pressure fluctuation data that is of interest regarding the free field stratosphere, and so they inherently corrupt the pressure fluctuation measurements. Furthermore, we could not decipher more information out of HAAT's acoustic data without access to other payloads, such as P10, in order to interrogate the acoustic frequencies of the motors and natural frequencies of the payload's structure. Had the hot-wire survived ground logistics, launch, and ascent, we would have been able to infer atmospheric disturbances in the pressure fluctuation data.

A Full Team Personnel

Table 16: Full team personnel.

Name	Start Date	End Date	Role	Student Status	Race	Ethnicity	Gender	Disabled
Matthew Killian	08/27/18	Present	Graduate Science Lead	Graduate	White	Non-Hispanic	Male	No
Cameron Storey	08/26/19	Present	Structural Lead	Undergrad	White	Non-Hispanic	Male	No
Jeremy Kuznetsov	08/30/21	Present	Mechanical Lead	Undergrad	White	Non-Hispanic	Male	No
Andrew Simone	08/30/21	Present	Electrical/Mechanical Subsystems	Undergrad	White	Non-Hispanic	Male	No
Saimah Siddiqui	08/31/20	Present	Electronics/Software Lead	Undergrad	Asian	Non-Hispanic	Female	No
Julianna Reese	08/30/21	Present	Electronics/Software Lead	Undergrad	White	Non-Hispanic	Female	No
Chaitanya Garg	08/30/21	Present	Thermal/Sensor integration	Undergrad	Asian	Non-Hispanic	Male	No
Alejandro Tovar	08/30/21	Present	Thermal Management Lead	Undergrad	White	Non-Hispanic	Male	No
Finnegan O'Neill	08/26/19	Present	Thermal and FEA Simulation Lead	Undergrad	White	Non-Hispanic	Male	No
Shaun Skinner	2018	Present	Project Manager (Post-Doc)	N/A	White	Non-Hipanic	Male	No
Mary Bowden	2000	Present	Faculty Advisory	N/A	White	Non-Hispanic	Female	No
Stuart Laurence	2013	Present	Faculty Advisory	N/A	White	Non-Hispanic	Male	No
Sonia Wharton	N/A	N/A	FDRCC Advisor	N/A	White	Non-Hispanic	Female	No
Alan Hidy	N/A	N/A	FDRCC Advisor	N/A	White	Non-Hispanic	Male	No
Tom Ehrmann	N/A	N/A	FDRCC Advisor	N/A	White	Non-Hispanic	Male	No

Table 17: Support team personnel.

Name	Start Date	End Date	Role	Student Status	Race	Eth-nicity	Gender	Dis-abled
Kruti Bhingradiya	08/31/20	Present	Mechanical and 3D printing	Undergrad	Asian	Non-Hispanic	Female	No
Maddie Lebetkin	08/28/19	Present	Mechanical	Undergrad	White	Non-Hispanic	Female	No
Michael Hoffman	08/31/20	Present	Mechanical	Undergrad	White	Non-Hispanic	Male	No
Kelly Deschaine	08/27/18	Present	Mechanical	Undergrad	White	Non-Hispanic	Female	No
Matt Griffin	08/27/18	Present	Aerosol Collection	Undergrad	White	Non-Hispanic	Male	No
Michael Kalin	08/27/19	Present	Electronics/Software	Undergrad	White	Non-Hispanic	Male	No
Sanya Doda	01/28/19	Present	Electronics/Software	Undergrad	Asian	Non-Hispanic	Female	No

Table 18: Key leadership personnel contact information.

Dr. Shaun Skinner	Project Manager	skinner1@umd.edu
Dr. Wenbo Zhu	Incoming PostDoc at UMD	zhu.1658@buckeyemail.osu.edu
Matthew Killian	Student Science Lead	mkillian@umd.edu
Dr. Mary Bowden	Faculty Advisor	bowden@umd.edu
Dr. Stuart Laurence	Faculty Advisor	stuartl@umd.edu
Dr. Sonia Wharton	FDRCC Advisor	wharton4@llnl.gov

B Technical Drawings

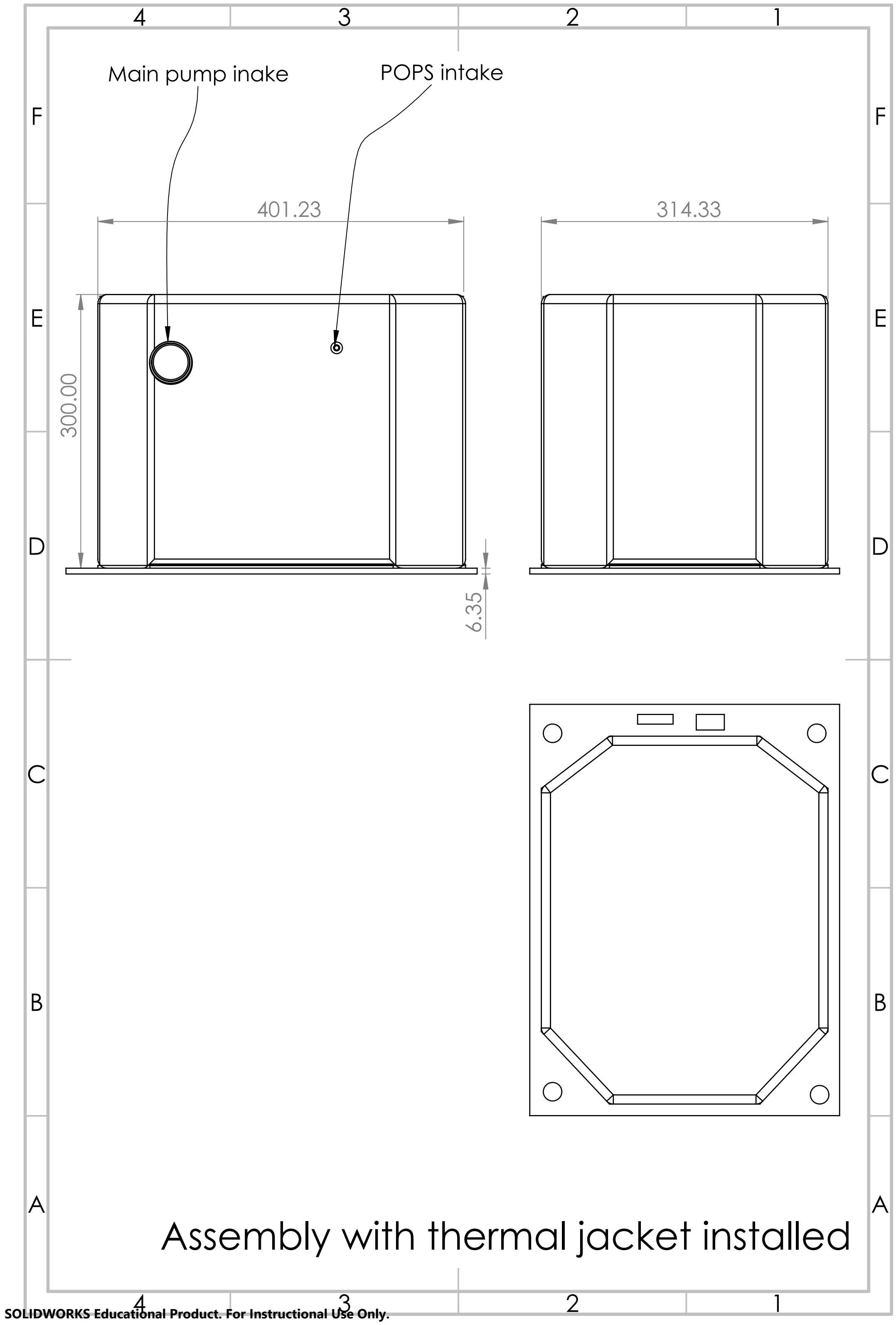

Figure 14: Schematic of payload on HASP mounting plate with thermal jacket INSTALLED and primary dimensions illustrated. Dimensions in mm.

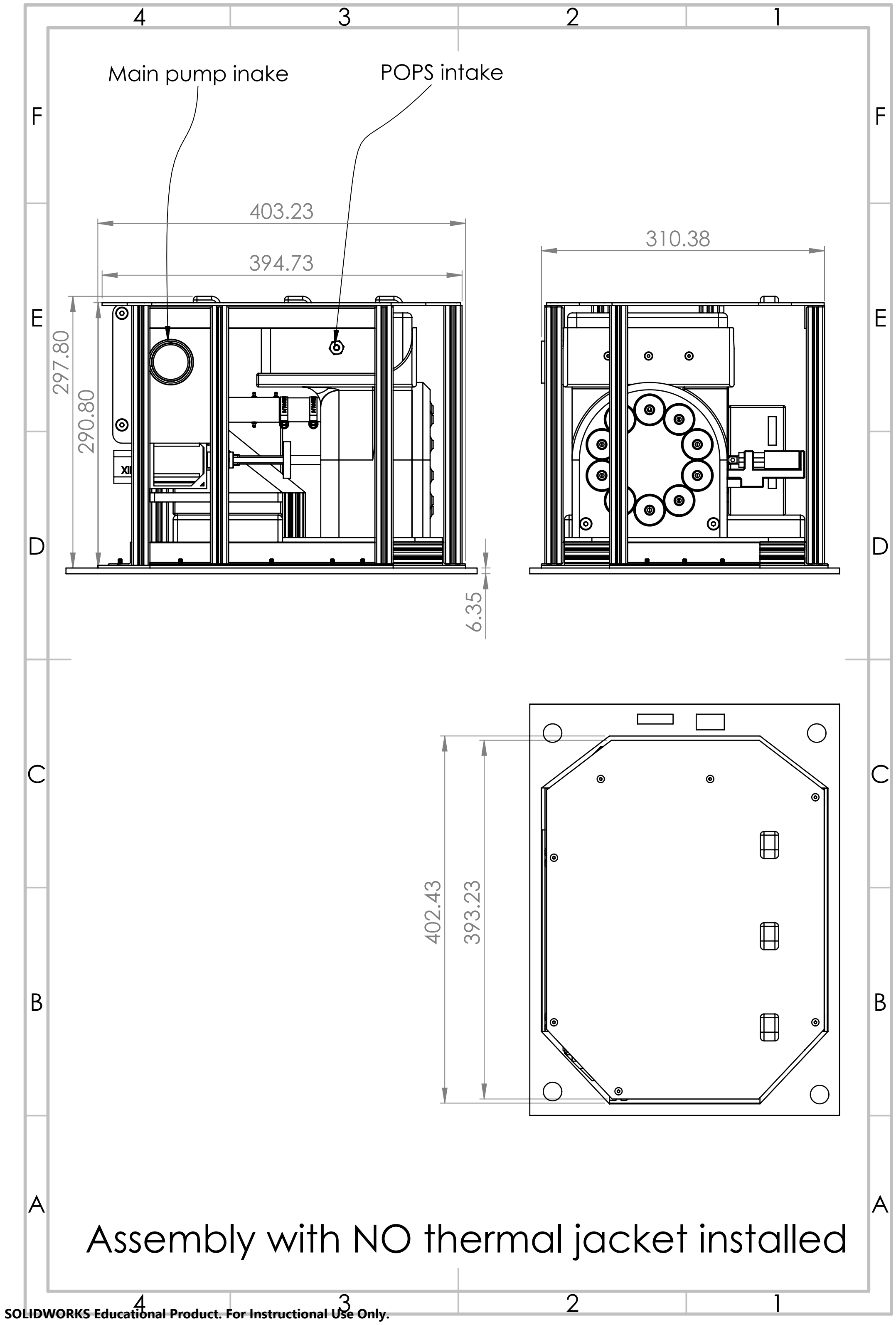

Figure 15: Schematic of payload on HASP mounting plate with thermal jacket REMOVED and primary dimensions illustrated. Dimensions in *mm*.

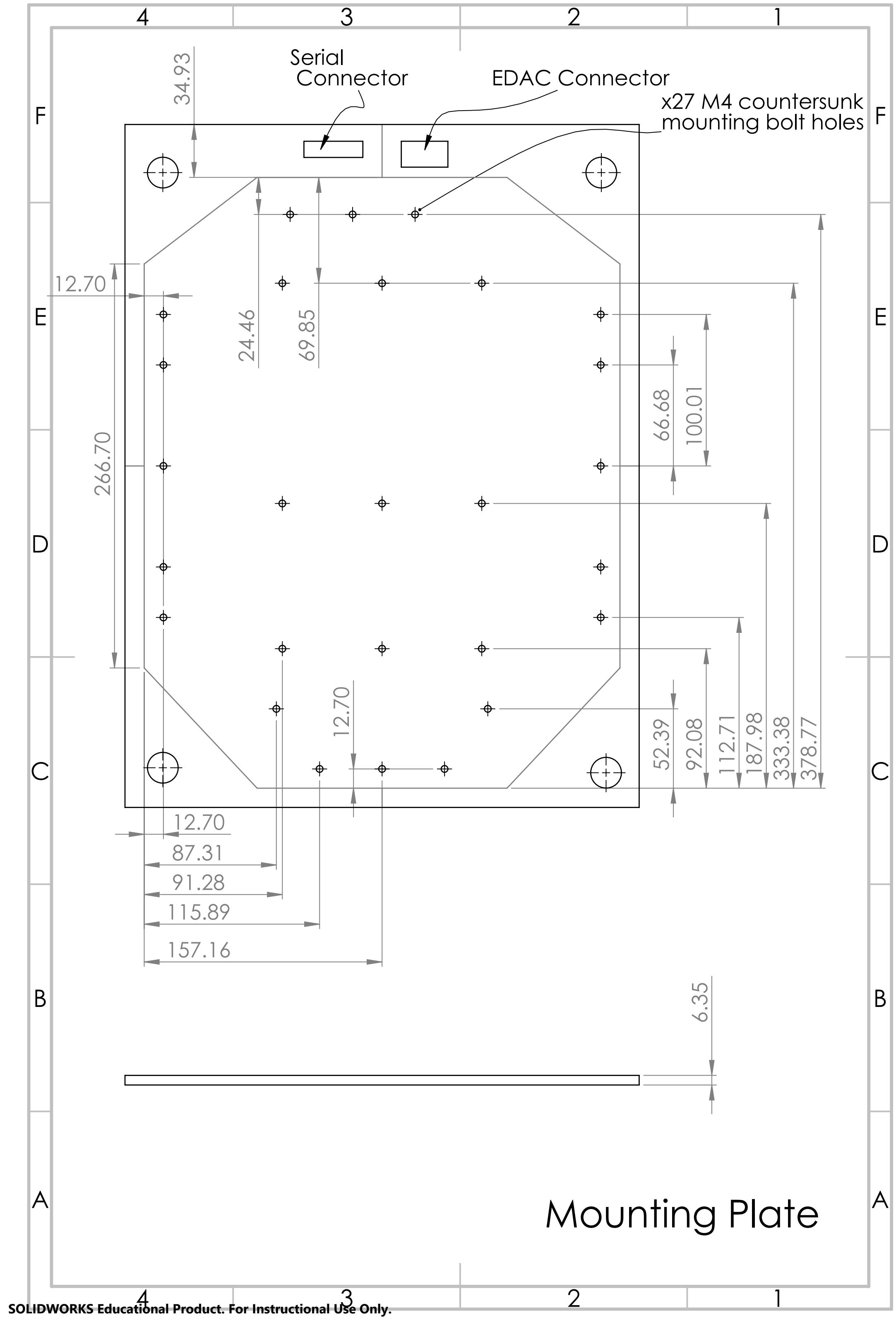

Figure 16: HASP 1/4" PVC mounting plate modifications; note that the footprint of the main GASP payload does not enter the 'Keep Out Area'. Dimensions in *mm*.

C Battery Hazard Documentation

Item	Units
Battery Manufacturer	Tenergy
Manufacturer Part No.	31892
Battery Type	Rechargeable battery pack (×8 18650 Cells)
Chemical Makeup	Chemistry Li-ion
Battery Modifications	**None**
UL Certification for 18650 Li-ion Battery Cell	*Attached*
Battery Charger Manual	*Attached*
Battery Web-page	*Attached*

Table 19: HASP 2022 Battery Hazard Documentation.

TENERGY

The Leader in Total Power Solution

Certificate of Compliance

436 Kato Terrace
Fremont, CA 94539
Tel: 510-687-0388
Fax: 510-687-0328

Product Description	Part Number	Material
Tenergy 3.6V 2600mAh 18650 Li-ion Battery Cell	30005-0	Lithium-ion (Cylindrical)

Tenergy hereby certifies that:
1) the product listed above meets the specifications and requirements listed in the production datasheet;

2) this product has been tested in accordance with the UL1642 standard and is UL-listed under file# MH48285 (model number LR1865SK).

Released by: Jun Xu Date: 03/29/2019

Signature: Xujun
Product Manager

Thank you for using Tenergy 4S/14.8V Li-ion/LiPo Charger!
Please read this manual before using the charger and operate as it instructs.

- Please DO NOT use this charger with any pack that doesn't have a built-in protection circuit board/module (PCB/PCM).
- Never use it for hobby packs (RC, airsoft, etc.) which are unprotected and are designed to be balance-charged.

Features:

- Smart charger for 4-cell 14.8V Li-ion and Li-Polymer battery pack with capacity>1500mAh.
- MCU controls the whole charging process to avoid over charge.
- Safety protection: over voltage protection, short circuit protection, reverse polarity protection, over current protection.
- Universal 100V- 240V AC input for worldwide power usage.
- 1500 mA constant charging current.
- Automatically stop charging when battery pack is fully charged.
- Output connector: Alligator clips.

Specifications:

Input voltage: 100VAC-240VAC 50HZ-60HZ;
Rated input current: 1000 mA
Battery type and specification: 4S/14.8V Li-ion/LiPo
Charging current: 1500mA
Charging voltage: 16.8V

Operation Instructions:

This is an easy-to-use charger. Just connect a battery to the charger, and make sure that the polarity is connected in the right way. Then connect the charger to AC power outlet.

LED Indicator:

Green:	Fully charged, and empty load
Red:	Charging
Flash:	Short circuit

Warning:

- Use special caution when working with Li-ion / Li-polymer cells and packs, they are very sensitive to charging characteristics and may explode if mishandled.
- Make sure user has enough knowledge on Li-ion rechargeable batteries in charging, discharging and assembly before use.
- Put the batteries in fire-proof environment in charging.
- Never leave batteries unattended when charging.
- Do not put batteries on car seat, wood surface or carpet when charging
- We are not responsible for any damage caused by misusing or mishandling, nor for any damage caused by other Li-ion batteries that are not supplied by Tenergy.
- Do not make any changes to the charger, charger accessories or connectors, as this might cause electrical shortage, fire or over-heating during charging.

AT: Tenergy Li-ion 18650 14.8V 5200mAh Rechargeable Battery Pack w/ PCB (4S2P, 76.96Wh, 6A Rate)

P/N 31892 |

BUILT-TO-ORDER ITEM

· Now! Build
Time: 3-7
ess Days

UCT
_IGHTS

- Chemistry Li-ion
- Nominal Voltage (V) 14.8
- Capacity (mAh) 5200
- Max Continuous Discharge Current 6A
- Weight 374g
- Dimension 73 x 73 x 37mm (LxWxT)
- Connector Bare Leads

Show Less

Price: $96.49
Instant Savings: $9.50

You Pay: **$86.99**

1 + -
ADD TO C/

Share:

D Laser Hazard Documentation

Item	Units
Manufacturer	Handix Scientific
Serial Number	*TBD*
GDFC ECN Number	*TBD*
Wavelength [nm]	405
Product Class	1
Laser Medium	Solid-State Laser Diode
Wave Type	*TBD*
Interlocks	Yes
Beam Shape	Gauss
Beam Diameter [mm]	< 1mm
Diameter at Waist [mm]	< 0.1mm
Beam Divergence [mrad]	*TBD*
Aperture to Waist Divergence [cm]	*TBD*
Major Divergence [mrad]	*TBD*
Minor Divergence [mrad]	*TBD*
PRF [Hz]	*TBD*
Average Power [mW]	70
Major Axis Dimension [mm]	*TBD*
Minor Axis Dimension [mm]	*TBD*
Pulse Width [sec]	*TBD*
Energy [Joules]	*TBD*
Gaussian Coupled [e-1, e-2]	*TBD*
Single Mode Fiber Diameter [mm]	*TBD*
Multi-Mode Fiber Diameter [mm]	NA

Table 20: HASP 2022 Laser Hazard Documentation.

References

[1] H. Ozawa, S.J. Laurence, J.M. Schramm, A. Wagner, and K. Hannemann. Fast-response temperature-sensitive-paint measurements on a hypersonic transition cone. *Experiments in Fluids*, 56(1):1–13, 2015.

[2] E. Reshotko. Boundary-Layer Stability and Transition. *Annual Review of Fluid Mechanics*, 8:311–349, 1976.

[3] W.M. Crooks, F.M. Hoblit, and F.A. Mitchell. Project HICAT: High Altitude Clear Air Turbulence Measurements and Meteorological Correlations. *Tech. Rep. AFFDL-TR-68-127, Air Force Flight Dynamics Lab*, 1, 1968.

[4] C.L. Johnson. Development of the Lockheed SR-71 Blackbird. *CIA Report 3675-81*, 1981.

[5] P.W. Merlin. Design and Development of the Blackbird: Challenges and Lessons Learned. In *47th AIAA Aerospace Sciences Meeting Including The New Horizons Forum and Aerospace Exposition: AIAA paper 2009-1522*, number January, 2009.

[6] Airbus and Perlan. Perlan Project Partners with Airbus Group to Fly a Glider to the Edge of Space: Press Release. *Perlan Project Inc.*, 2014.

[7] Airbus and Perlan. Airbus Perlan Mission II Glider Soars to 76,000 feet to Break Own Altitude Record, Surpassing Even U-2 Reconnaissance Plane: Press Release. *Perlan Project Inc.*, 2018.

[8] D. Cadet. Energy dissipation within intermittent clear air turbulence patches. *Journal of the Atmospheric Sciences*, 34:137–142, 1977.

[9] J. Barat. Some characteristics of clear-air turbulence in the middle stratosphere. *Journal of the Atmospheric Sciences*, 39:2553–2564, 1982.

[10] J. Barat, C. Cot, and C. Sidi. On the measurement of turbulence dissipation rate from rising balloons. *Journal of Atmospheric and Oceanic Technology*, 1:270–275, 1984.

[11] A. Theuerkauf. *Stratospheric turbulence observations with the new balloon-borne instrument LITOS*. PhD thesis, University of Rostock, 2012.

[12] A. Schneider, J. Wagner, J. Söder, M. Gerding, and F.J. Lübken. Case study of wave breaking with high-resolution turbulence measurements with LITOS and WRF simulations. *Atmospheric Chemistry and Physics*, 17(12):7941–7954, 2017.

[13] F.J. Lübken, W. Hillert, G. Lehmacher, and U. von Zahn. Neutral air turbulence during DYANA: First results. *Advances in Space Research*, 12(10):135–139, 1992.

[14] S. Skinner, C. Butler, S.J. Laurence, and A. Mangalam. In-Situ Measurements of Turbulent Velocity, Temperature, and Acoustic Fluctuations in the Stratosphere. *AIAA SciTech 2020*, 2020.

[15] C. Jordan, J.E. Dibb, and H. Fuelberg. Uptake of nitrate and sulfate on dust aerosols during TRACE-P. *Journal of Geophysical Research*, 108(D21), 2003.

[16] D. Koch and D. Rind. Beryllium 10/beryllium 7 as a tracer of stratospheric transport. *Journal of Geophysical Research*, 103:3907–3917, 1998.

[17] D. Lal and B. Peters. Cosmic Ray Produced Isotopes and their Application to Problems in Geophysics. *Progr. Elem. Particle Cosmic Ray Phys.*, 6, 1962.

[18] N. Bhandri, D. Lal, and Rama. Stratospheric circulation studies based on natural and artificial radioactive tracer elements . *Tellus*, 18:391–406, 1966.

[19] L.R. McHargue and P.E. Damon. The global beryllium 10 cycle. *Reviews of Geophysics*, 29(2):141–158, 1991.

[20] E.F. Danielsen and R.S. Hipskind. High Resolution Vertical Profiles of Wind, Temperature, and Humidity Obtained by Computer Processing and Digital Filtering of Radiosonde and Radar Tracking Data From the ITCZ Experiment of 1977. *NASA contractor Report 3269*, 1980.

[21] M.A Kritz, S.W. Rosner, Danielsen E.F., and H.B. Selkirk. Air Mass Origins and Troposphere-to-Stratosphere Exchange Associated with Mid-Latitude Cyclogenesis and Tropopause Folding Inferred from 7Be Measurements. *Journal of Geophysical Research: Atmospheres*, 96(17):405–417, 1991.

[22] J.E. Dibb, D. Meeker, R.C. Finkel, and J Southon. Estimation of Stratospheric Input to the Arctic Troposphere: 7Be and 10Be in aerosols at Alert, Canada. *Journal of Geophysical Research*, 99(17):12855–12865, 1994.

[23] J.E. Dibb, R.W. Talbot, and E. Scheuer. Asian Influence over the Western North Pacific During the Fall Season: Inferences from Lead 210, Soluble Ionic Species and Ozone. *Journal of Geophysical Research: Atmospheres*, 101(D3):1779–1792, 1996.

[24] J.E. Dibb, R.W. Talbot, B.L. Lefer, E. Scheuer, G.L. Gregory, E.V. Browell, J.D. Bradshaw, S.T. Sandholm, and H.B. Singh. Distributions of Beryllium 7 and Lead 2109, and Soluble Aerosol-Associated Ionic Species Over the Western Pacific: PEM West B, February-March 1994. *Journal of Geophysical Research*, 102(17):28287–28302, 1997.

[25] J.E. Dibb, R.W. Talbot, and E. . Scheuer. Composition and distribution of aerosols over the North Atlantic during the Subsonic Assessment Ozone and Nitrogen Oxide Experiment (SONEX). *Journal of Geophysical Research: Atmospheres*, 2000.

[26] S. Rehfeldd and M. Heimann. Three Dimensional Atmospheric Transport Simulation of the Radioactive Rracers 210Pb, 7Be, 10Be, and 90Sr. *Journal of Geophysical Research*, 1996.

[27] G. Delaygue, S. Bekki, and E. Bard. Modelling the Stratospheric Budget of Beryllium Isotopes. *Chemical and Physical Meteorology*, 67(1), 2015.

[28] A. Stohl, P. Bonasoni, W. Cristofanelli, and et al. Feichter. Stratosphere-troposphere exchange: A review, and what we have learned from STACCATO. *Journal of Geophysical Research*, 108(D12), 2003.

[29] J. Hoogheim, M. Vries, H. Been, P. Hekkinen, R. Kivi, and H. Chen. LISA: a lightweight stratospheric air sampler. *Atmospheric Measurement Techniques*, 11(12):6785–6801, 2018.

[30] NASA. HASP – Student Payload Interface Manual; Version 02.17.09. Technical report, 2022.